

1

Improved Treatment of Dark Matter Capture in Compact Objects

Review capture in the Sun, move to what's needed for COs in general, then specify to WDs (ions + electrons) and NS (interacting baryons)

The capture rate of dark matter within celestial bodies is an essential quantity of interest throughout this work. In this chapter, we focus on building up the formalism of dark matter capture within compact objects, outlining how this differs from the established formalism for capture in the Sun. We restrict our analysis to scattering off of point-like targets relevant for leptonic species, i.e. electrons in White Dwarfs and electrons and muons in Neutron Stars, though much of the formalism is introduced with neutron targets.

1.1 Dark Matter Capture in the Sun

Before jumping into the capture formalism relevant to compact objects, it will serve us well to review the formalism laid out by Gould for capture in the Sun [1, 2].

To begin, we consider the flux of dark matter particles that pass through a spherical shell a large distance R from the star, where the gravitational field is negligible. For this, we need to know the distribution function of the relative velocity between the DM and the stellar constituents. The velocity distribution function will be spatially isotropic, and so for simplicity we will assume that the

DM follows a Maxwell-Boltzmann distribution function,

$$f_\infty(\tilde{u}_\chi)d\tilde{u}_\chi = 4\pi \left(\frac{3}{2\pi}\right)^{3/2} \frac{\tilde{u}_\chi^2}{v_d^2} \exp\left(-\frac{3\tilde{u}_\chi^2}{2v_d^3}\right) d\tilde{u}_\chi, \quad (1.1)$$

where \tilde{u}_χ is the DM velocity in the halo, and v_d is the DM halo velocity dispersion.

Taking into account the motion of the star through the halo and the thermal motion of the constituents, which are assumed to follow a Maxwell-Boltzmann distribution, gives the relative velocity between the DM and targets, u_χ . The distribution function for the relative velocity can be expressed as [3]

$$f_{\text{MB}}(u_\chi)du_\chi = \frac{u_\chi}{v_\star} \sqrt{\frac{3}{2\pi(v_d^2 + 3T_\star/m_i)}} \left(e^{-\frac{3(u_\chi - v_\star)^2}{2(v_d^2 + 3T_\star/m_i)}} - e^{-\frac{3(u_\chi + v_\star)^2}{2(v_d^2 + 3T_\star/m_i)}} \right), \quad (1.2)$$

where v_\star is the star's velocity in the halo rest frame¹, T_\star is the temperature of the star, and m_i is the mass of the target.

Returning to the large spherical shell of radius R , given the velocity distribution function, we can obtain the flux of DM through this surface. The rate of DM particles passing through a surface element $d\tilde{A}$ with velocity between u_χ and $u_\chi + du_\chi$, with an angle to the normal of $d\tilde{A}$ between $\tilde{\theta}$ and $\tilde{\theta} + d\tilde{\theta}$ and an azimuthal angle between $\tilde{\phi}$ and $\tilde{\phi} + d\tilde{\phi}$ is given by [4]

$$\frac{dN_\chi}{dt} = \frac{\rho_\chi}{m_\chi} f_{\text{MB}}(u_\chi) \vec{u} \cdot d\tilde{A} du_\chi \frac{d\tilde{\Omega}}{4\pi} \quad (1.3)$$

$$= \frac{\rho_\chi}{m_\chi} f_{\text{MB}}(u_\chi) u_\chi \cos \tilde{\theta} d\tilde{A} du_\chi \frac{d \cos \tilde{\theta} d\tilde{\phi}}{4\pi} \quad (1.4)$$

$$= \frac{1}{4} \frac{\rho_\chi}{m_\chi} f_{\text{MB}}(u_\chi) u_\chi d\tilde{A} du_\chi d \cos^2 \tilde{\theta}, \quad (1.5)$$

where we have integrated over the azimuthal angle $\tilde{\phi}$ due to the isotropy of the system. The number density of the DM is included through the ρ_χ/m_χ factor. Integrating over the area of the sphere is trivial due to isotropy, leaving us with

$$\frac{dN_\chi}{dt} = \pi \frac{\rho_\chi}{m_\chi} f(u_\chi) u_\chi du_\chi d \cos^2 \tilde{\theta}, \quad (1.6)$$

with the integration interval for $\cos^2 \tilde{\theta}$ being $(0, 1)$.

As the DM begins to infall from this large distance R to a closer distance r , the star's gravitational field will boost the velocity by the local escape velocity $v_e(r)$

¹This is the frame where the DM has an average velocity of zero.

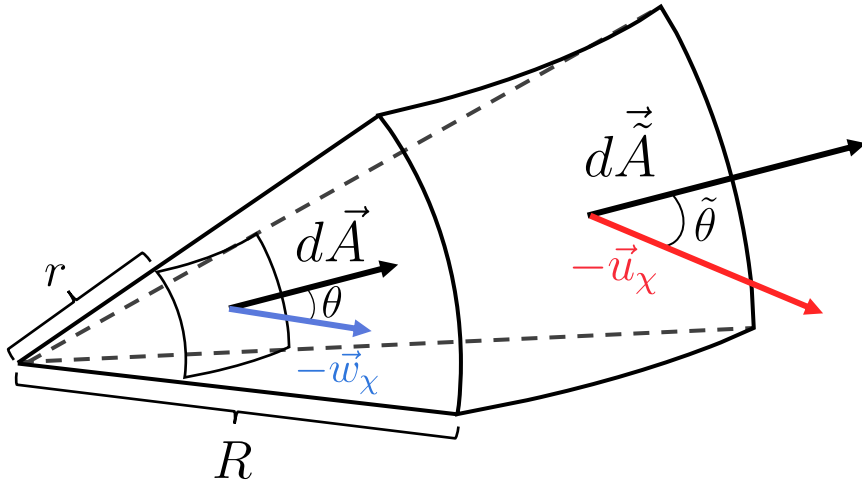


Figure 1.1: Geometry of the capture process, showing two elements of spheres with radii r close to the star

such that

$$w_\chi^2(r) = u_\chi^2 + v_e^2(r), \quad (1.7)$$

$$v_e^2(r) = \frac{2GM_\star}{R_\star} + \int_r^{R_\star} \frac{GM_\star(r')}{r'^2} dr'. \quad (1.8)$$

Due to the conservation of angular momentum, we can relate the angular momentum of the DM at the two distances R and r such that

$$J_\chi = m_\chi Ru_\chi \sin \tilde{\theta} = m_\chi rw_\chi(r) \sin \theta \leq m_\chi rw_\chi(r) \equiv J_{\max}, \quad (1.9)$$

where θ is the incident angle of the DM at the closer distance r , and we have defined the maximum angular momentum J_{\max} corresponding to a linear DM trajectory.

Changing integration variables from $\cos^2 \tilde{\theta}$ to J_χ allows us to write the number of DM particles passing through the shell per unit volume as

$$\frac{dN_\chi}{dt} = 2\pi \frac{\rho_\chi}{m_\chi} \frac{f_{\text{MB}}(u_\chi)}{u_\chi} r^2 w_\chi^2(r) \frac{J_\chi dJ_\chi}{J_{\max}^2} du_\chi. \quad (1.10)$$

The geometry of the system is shown in Fig. 1.1 for clarity.

The probability that the DM interacts with the constituents of the shell depends on the interaction rate, $\Omega(w_\chi)$, multiplied by the time spent in the shell, $dt = dr/\dot{r}$.

Hence, the probability of scattering within the shell is

$$\Omega(w_\chi) \frac{dr}{\dot{r}} = 2\Omega(w_\chi) \frac{1}{w_\chi} \left(1 - \left(\frac{J_\chi}{rw_\chi} \right)^2 \right)^{-1/2} \Theta(J_{\max} - J_\chi) dr, \quad (1.11)$$

where the factor of 2 is due to the DM having two opportunities to pass through the shell, once when incoming and another after turning around². The step-function is put in to ensure the angular momentum does not exceed its maximum allowed value.

For a scattered DM to be considered captured, it must lose enough energy in the collision to become gravitationally bound. The rate at which a DM particle scatters from an initial velocity w_χ to a final velocity $v < v_e(r)$ is given by [1–3]

$$\Omega^-(w_\chi) = \int_0^{v_e} R^-(w_\chi \rightarrow v) dv, \quad (1.12)$$

$$R^-(w_\chi \rightarrow v) = \int n_T(r) \frac{d\sigma_{\chi T}}{dv} |\vec{w}_\chi - \vec{u}_T| f_T(u_T) d^3 \vec{u}_T, \quad (1.13)$$

with $R^-(w_\chi \rightarrow v)$ being the differential interaction rate, n_T is the target number density, u_T is the target velocity and $f_T(u_T)$ is the corresponding distribution function, and $d\sigma_{\chi T}/dv$ is the differential cross-section. The minus superscript is used to signify that this is the down scattering rate, i.e. the rate of interactions leading to the DM losing energy.

Finally, we obtain the capture rate by multiplying Eqs. 1.10 and 1.11 and integrate over the angular momentum to give the result

$$C = \int_0^{R_*} dr 4\pi r^2 \int_0^\infty du_\chi \frac{\rho_\chi}{m_\chi} \frac{f_{\text{MB}}(u_\chi)}{u_\chi} w_\chi(r) \Omega^-(w_\chi). \quad (1.14)$$

This result is rather generic, as the choice of DM model will only dictate the form of the differential cross-section in Eq. 1.13. As written above, the distribution function for the relative velocity far from the star can be any isotropic distribution function. The MB form was chosen as it allows for a simple analytic form of the total capture rate.

1.2 Capture in Compact Objects

Having reviewed the capture process in non-relativistic stars, we can begin discussing the necessary modifications required when considering relativistic stars. In this section, we consider the two major modifications that need to be made:

²The radial velocity \dot{r} is a standard result in orbital mechanics and can be obtained from the central force Lagrangian.

- The corrections from General Relativity due to the extreme gravitational fields. This ultimately alters the flux of DM passing through the star, boosting it through gravitational focusing.
- Accounting for the relativistic and degenerate nature of the star's constituents in the interaction rate.

The former is generic to neutron stars and white dwarfs, while the latter is required for all NS constituents, but only the electrons in a WD are degenerate and relativistic. The ions of the WD are non-relativistic and non-degenerate and, hence, can the solar capture formalism can be applied in this case.

1.2.1 General Relativistic Corrections to the Capture Rate

Far from the star, the physics is the same as in the previous section. The deviations arise as the DM falls into the gravitational potential of the star. We begin by following the DM along its trajectory, moving from a distance $R \gg R_\star$ to a closer distance r . Hence, we are working in the DM rest frame and calculating the rate at which the DM passes through the shell *per unit of proper time*, τ . The proper time interval is related to the metric through

$$d\tau^2 = B(r)dt^2 - A(r)dr^2 - r^2d\Omega^2, \quad (1.15)$$

with $B(r)$ and $A(r)$ defined in Chapter ??.

Following the same arguments as in the non-relativistic case, the flux of DM passing through the shell is

$$\frac{dN_\chi}{d\tau} = 2\pi \frac{\rho_\chi}{m_\chi} \frac{f_{\text{MB}}(u_\chi)}{u_\chi} du_\chi \frac{J_\chi dJ_\chi}{m_\chi^2}, \quad (1.16)$$

which takes the same form as Eq. 1.10, with the physical difference being that this is the rate with respect to the proper time.

The probability that DM scatters within the shell and is captured is $2\hat{\Omega}^-(r)d\tau$, where $\hat{\Omega}^-(r)$ is the interaction rate with respect to the proper time, and $d\tau$ is the proper time taken to move from coordinate r to $r + dr$. The factor of 2 once again accounts for the DM crossing the shell twice per orbit. For calculation purposes, we need to relate this to the interaction rate seen by a distant observer, $\Omega^-(r)$, that is done through

$$\hat{\Omega}^-(r)d\tau = \frac{1}{\sqrt{g_{tt}}} \Omega^-(r)d\tau = \frac{1}{\sqrt{B(r)}} \Omega^-(r)d\tau. \quad (1.17)$$

Now, the proper time that the DM spends inside a shell of thickness dr will be³

$$d\tau = \left(\frac{d\tau}{dt} \right) dt = B(r) \frac{dr}{\dot{r}} = \frac{\sqrt{B(r)} dr}{\sqrt{\frac{1}{A(r)} \left[1 - B(r) \left(1 + \frac{J_\chi^2}{m_\chi^2 r^2} \right) \right]}}. \quad (1.18)$$

The differential capture rate can then be written as

$$dC = 2\pi \frac{\rho_\chi}{m_\chi} \frac{f_{\text{MB}}(u_\chi)}{u_\chi} du_\chi \frac{dJ_\chi^2}{m_\chi^2} \frac{\Omega^-(r) \sqrt{A(r)} dr}{\sqrt{1 - B(r) \left(1 + \frac{J_\chi^2}{m_\chi^2 r^2} \right)}}. \quad (1.19)$$

As the total number of targets in the star, N_T , needs to satisfy

$$N_T = \int_0^{R_*} 4\pi r^2 n_T(r) \sqrt{A(r)} dr, \quad (1.20)$$

where $n_T(r)$ is the number density that appears in the interaction rate, we absorb the factor $\sqrt{A(r)}$ into the definition of $n_T(r)$, such that $\Omega^-(r) \sqrt{A(r)} \rightarrow \Omega^-(r)$. This is due to the number densities obtained by solving the TOV equations already account for the $\sqrt{A(r)}$ factor.

As before, we have $w_\chi^2(r) = u_\chi^2 + v_e^2(r)$, however as the escape velocity will be significantly larger than the ambient DM velocity far from the star, we can safely approximate $w_\chi^2(r) \approx v_e^2(r)$. In the relativistic case, the escape velocity can be defined as

$$v_e^2(r) = \left(\frac{dl}{d\tau} \right)^2 = A(r) \left(\frac{dr}{d\tau} \right)^2 + r^2 \left(\frac{d\phi}{d\tau} \right)^2 = 1 - B(r), \quad (1.21)$$

where dl is a length element. The large boost from the escape velocity also removes the u_χ dependence in the kinematics of the interactions and allows us to perform the integration over the initial DM velocity, yielding an overall factor of

$$\int_0^\infty \frac{f_{\text{MB}}(u_\chi)}{u_\chi} du_\chi = \frac{1}{v_\star} \text{Erf} \left(\sqrt{\frac{3}{2}} \frac{v_\star}{v_d} \right). \quad (1.22)$$

To integrate over J_χ^2 , we need the maximum angular momentum the DM can achieve as it passes through the shell. This can be obtained by requiring the argument of the radical above to remain positive, giving

$$J_{\max} = \sqrt{\frac{1 - B(r)}{B(r)}} m_\chi r. \quad (1.23)$$

³See Appendix ?? for the derivation of $\dot{r} = \frac{dr}{dt}$.

The factor of $1/\sqrt{B}$ arises due to the gravitational focusing of the incoming flux of DM [5].

Putting everything together, and integrating over the radius of the star, we are left with the final result for the capture rate of

$$C = \frac{4\pi}{v_\star} \frac{\rho_\chi}{m_\chi} \operatorname{Erf} \left(\sqrt{\frac{3}{2}} \frac{v_\star}{v_d} \right) \int_0^{R_\star} r^2 \frac{\sqrt{1 - B(r)}}{B(r)} \Omega^-(r) dr. \quad (1.24)$$

All that remains is determining the form of the interaction rates for relativistic energies.

1.2.2 Geometric Limit and Threshold Cross-Section

In the previous section, we derived an expression for the capture rate assuming that the DM is captured after a single scatter, and that it only scatters once along its orbit through the NS. This first assumption is true for DM light enough to lose enough energy in this single interaction, which for nucleon targets turns out to be $m_\chi \lesssim 10^6$ GeV. The latter assumption is a statement that we are working in the optically thin regime, such that the cross-section is much less than the “threshold cross-section”, σ_{th} . The value of the threshold cross-section is defined as the cross-section for which the capture rate evaluated in the optically thin regime is equal to the geometric limit [6],

$$C_{\text{geom}} = \frac{\pi R_\star^2 (1 - B(R_\star))}{v_\star B(R_\star)} \frac{\rho_\chi}{m_\chi} \operatorname{Erf} \left(\sqrt{\frac{3}{2}} \frac{v_\star}{v_d} \right). \quad (1.25)$$

This is the capture rate for which the entire flux of DM passing through the surface of the star is captured at the surface. Hence, it serves as an upper bound to the capture rate, with cross-sections greater than σ_{th} saturating the capture rate to this value. Note the $1/B(R_\star)$ factor in the equation above. In stars and planets where classical Newtonian mechanics can be applied, gravitational focusing would result in a factor $v_{\text{esc}}^2/v_\star = (1 - B(R_\star))/v_\star$ in Eq. 1.25, where we have used Eqs. 1.21 and ???. In neutron stars, on the other hand, general relativity introduces an additional factor of $1/B(R_\star)$, which can be obtained from the derivation of the flux of DM particles accreted to a NS with a Schwarzschild metric (Eq. 1.24) [5, 7].

For scattering on neutrons, the threshold cross-section is approximately

$$\sigma_{\text{th}} = \begin{cases} \sigma_{\text{ref}} \frac{\text{GeV}}{m_\chi} & m_\chi \lesssim 1 \text{ GeV} \quad \text{Pauli blocking regime,} \\ \sigma_{\text{ref}} & 1 \text{ GeV} \lesssim m_\chi \lesssim 10^6 \text{ GeV,} \\ \sigma_{\text{ref}} \frac{m_\chi}{10^6 \text{ GeV}} & m_\chi \gtrsim 10^6 \text{ GeV} \quad \text{Multiscattering regime,} \end{cases} \quad (1.26)$$

where we take the canonical value of

$$\sigma_{\text{ref}} \sim 1.7 \times 10^{-45} \text{ cm}^2, \quad (1.27)$$

which assumes the NS is a solid sphere such that $\sigma_{\text{ref}} \sim m_n \pi R_\star^2 / M_\star$ with m_n the neutron mass.

For scattering off other targets, Pauli blocking is relevant for $q_0^{\text{MAX}} \lesssim \mu_{\text{target}}$ while multi-scattering is relevant for $m_\chi \gtrsim q_0^{\text{MAX}} / v_\star^2$, where q_0^{MAX} is the maximum energy transferred in a collision, as will be discussed later. In addition, because the other target species have a lower abundance than neutrons, the reference cross-section, σ_{ref} , will be higher. The values of σ_{th} in Eq. 1.26, and their regions of applicability, can thus be altered appropriately for other target species of interest.

1.2.3 Interaction Rate for Relativistic Energies and Degenerate Targets

Our next goal is to write down an interaction rate suitable for describing the interactions between relativistic particles and account for the degeneracy of the target species. This will be achieved by modifying the non-relativistic interaction rate of Eq. 1.12 through the use of relativistic kinematics and the use of Lorentz invariant quantities, and the correct distribution functions for degenerate fermion targets.

As shown in Eqs. 1.12 and 1.13, the interaction rate between non-relativistic, non-degenerate species i can be expressed as

$$\Omega^-(r) = \int dv \frac{d\sigma}{dv} |\vec{w}_\chi - \vec{u}_i| n_i(r) f_{\text{MB}}(u_i) d^3 u_i. \quad (1.28)$$

First, we address the degeneracy of the targets by exchanging the Maxwell-Boltzmann distribution function for a Fermi-Dirac (FD) distribution, $f_{\text{FD}}(E_i, r)$, via the replacement

$$n_i(r) f_{\text{MB}}(u_i) d^3 u_i \rightarrow \frac{g_s}{(2\pi)^3} f_{\text{FD}}(E_i, r), \quad (1.29)$$

where $g_s = 2$ is the number of spin states of the target species, p is the 3-momentum of the incoming target, and E_i is its corresponding energy. The radial dependence of the FD distribution stems from its implicit dependence on the chemical potential of the target. Rewriting this expression in a more computationally friendly manner in terms of the relevant kinematic quantities results in

$$\frac{g_s}{(2\pi)^3} f_{\text{FD}}(E_i, r) = \frac{p E_i}{2\pi^2} f_{\text{FD}}(E_i, r) dE_i d\cos\theta_{uw}, \quad (1.30)$$

where we have expressed the angular component of the d^3p differential in terms of the angle between the incoming DM and target. This angle can be traded for the more useful quantity s , the centre of mass energy through

$$\frac{d \cos \theta_{uw}}{ds} = \frac{1}{2pp_\chi} = \frac{1}{2p\sqrt{E_\chi^2 - m_\chi^2}} = \frac{1}{2pm_\chi} \sqrt{\frac{B(r)}{1 - B(r)}}, \quad (1.31)$$

as the initial DM energy is $E_\chi = m_\chi / \sqrt{B(r)}$.

Next, we calculate the initial relative velocity, $|\vec{w}_\chi - \vec{u}_i|$, using relativistic kinematics, expressing it in terms of the Mandelstam s ,

$$|\vec{w}_\chi - \vec{u}_i| = \frac{\sqrt{s^2 - 2s(1 + \mu^2)m_i^2 + (1 - \mu^2)^2m_i^4}}{s - (1 + \mu^2)m_i^2}, \quad (1.32)$$

where $\mu = m_\chi/m_i$.

Given that it is most common to present the relativistic differential scattering cross-section $d\sigma/d \cos \theta_{cm}$ as a function of the Mandelstam variables s and t , with θ_{cm} the centre of mass frame scattering angle, we make the replacement

$$dv \frac{d\sigma}{dv} = dt \frac{d\sigma}{dt} = dt \frac{d\sigma}{d \cos \theta_{cm}} \frac{d \cos \theta_{cm}}{t}. \quad (1.33)$$

The final Jacobian factor can be expressed as

$$\frac{d \cos \theta_{cm}}{dt} = \frac{2s}{s^2 - 2s(1 + \mu^2)m_i^2 + (1 - \mu^2)^2m_i^4}, \quad (1.34)$$

for the elastic scattering we consider here.

Finally, we note that the first application of this capture formalism was for neutron targets, with the analysis completed before we had considered the additional effects from the form factors and strong interactions discussed in subsection ???. These effects will be incorporated into this formalism in a self-consistent way next chapter. The initial approach that was taken to account for the fact that we are using realistic neutron number density profiles, despite the expression in Eq. 1.29 being for a free Fermi gas, is to introduce a correction factor as in Ref. [8],

$$\zeta(r) = \frac{n_i(r)}{n_{free}(r)}, \quad (1.35)$$

where $n_{free}(r)$ is obtained by integrating Eq. 1.30 over all phase space. In the zero-temperature approximation, the result is

$$n_{free}(r) = \frac{1}{3\pi^2} [\varepsilon_{F,i}(r)(2m_i + \varepsilon_{F,i}(r))]^{3/2}. \quad (1.36)$$

Compiling everything together leads to the final expression for the interaction rate being

$$\Omega^-(r) = \int dt dE_i ds \zeta(r) \frac{d\sigma}{d \cos \theta_{\text{cm}}} \frac{E_i}{2\pi^2 m_i} \sqrt{\frac{B(r)}{1 - B(r)}} \frac{s}{\beta(s)\gamma(s)} \times f_{\text{FD}}(E_i, r)(1 - f_{\text{FD}}(E'_i, r)), \quad (1.37)$$

where we have introduced the helper functions

$$\beta(s) = s - (m_i^2 + m_\chi^2), \quad (1.38)$$

$$\gamma(s) = \sqrt{\beta^2(s) - 4m_i^2 m_\chi^2}. \quad (1.39)$$

We have also introduced the Pauli blocking factor, $1 - f_{\text{FD}}(E'_i, r)$, to account for the phase space available to the final state target. The energy of this final state particle, E'_i , is in general a messy function of E_i , t , s , and r , and can be obtained from the kinematics of the scattering. This result is presented in Appendix ??.

The integration intervals are

$$t_{\min} = -\frac{\gamma(s)}{s}, \quad (1.40)$$

$$t_{\max} = 0, \quad (1.41)$$

$$s_{\min} = m_i^2 + m_\chi^2 + 2\frac{E_i m_\chi}{\sqrt{B(r)}} - 2m_\chi \sqrt{\frac{1 - B(r)}{B(r)}} \sqrt{E_i^2 - m_i^2}, \quad (1.42)$$

$$s_{\max} = m_i^2 + m_\chi^2 + 2\frac{E_i m_\chi}{\sqrt{B(r)}} + 2m_\chi \sqrt{\frac{1 - B(r)}{B(r)}} \sqrt{E_i^2 - m_i^2}, \quad (1.43)$$

$$E_{i,\min} = m_i, \quad (1.44)$$

$$E_{i,\max} = \frac{m_i}{\sqrt{B(r)}}. \quad (1.45)$$

As we will be dealing with NSs at low temperatures, we can take the $T_\star \rightarrow 0$ limit and replace the FD functions with step functions,

$$f_{\text{FD}}(E_i, r) \rightarrow \Theta(\varepsilon_{F,i}(r) + m_i - E_i), \quad (1.46)$$

$$1 - f_{\text{FD}}(E'_i, r) \rightarrow \Theta(E'_i - m_i - \varepsilon_{F,i}(r)). \quad (1.47)$$

The first step function can be used to further restrict the E_i integration interval to be $[m_i, m_i + \varepsilon_{F,i}(r)]$. In practice, we work with the kinetic energies of the targets rather than their total energy, as this is the quantity that directly changed in the interactions. Therefore, unless otherwise specified, we will take E_i to mean the target kinetic energy, with the integration range being $0 \leq E_i \leq \varepsilon_{F,i}$.

This expression resembles that of Ref. [8], but uses a relativistic formalism instead. In Appendix ??, we show that Eq. 1.37 reduces to the classical expression for the interaction rate in the non-relativistic limit.

1.3 The Differential Interaction Rate

In the previous section, we have calculated the interaction rate, $\Omega^-(r)$, assuming the initial DM energy takes its pre-capture value, $E_\chi = m_\chi/B(r)$. However, we are also interested in an expression for the interaction rate valid for arbitrary DM energy. This will be required when we consider capture via multiple scatterings, and it will also be necessary to study the subsequent scattering interactions that follow capture and lead to the DM thermalising within the NS. In principle, it is possible to calculate this rate numerically by binning Ω^- , Eq. 1.37, in the energy loss, i.e. multiplying Ω^- by $\frac{1}{E_i - E_j} \Theta(E_i + E_i - E'_i) \Theta(E'_i - E_i - E_j)$ and integrating over the bin $[E_j, E_i]$. However, it is possible to derive analytic expressions for the differential rate, valid in the zero-temperature approximation. To do so, we use the definition of the scattering rate in Ref. [9, 10]

$$\Gamma^-(E_\chi) = 2 \int \frac{d^3 k'}{(2\pi)^3} \int \frac{d^3 p}{(2\pi)^3} \int \frac{d^3 p'}{(2\pi)^3} \frac{|\bar{\mathcal{M}}|^2}{(2E_\chi)(2E'_\chi)(2E_i)(2E'_i)} (1.48)$$

$$\times (2\pi)^4 \delta^4(k_\mu + p_\mu - k'_\mu - p'_\mu) f_{\text{FD}}(E_i)(1 - f_{\text{FD}}(E'_i)),$$

where $|\bar{\mathcal{M}}|^2$ is the squared matrix element, $k^\mu = (E_\chi, \vec{k})$ and $k'^\mu = (E'_\chi, \vec{k}')$ are the DM initial and final momenta, and $p^\mu = (E_i, \vec{p})$ and $p'^\mu = (E'_i, \vec{p}')$ are the target particle initial and final momenta, respectively. To see that Γ^- is indeed the same as Ω^- in Eq. 1.37, multiply and divide by $v_{\text{rel}} = |\vec{w} - \vec{u}_i|$ to reintroduce the quantum field theoretic definition of differential cross-section,

$$d\sigma = \frac{|\bar{\mathcal{M}}|^2}{2E_\chi 2E_i |\vec{w} - \vec{u}_i|} d^2\Pi_{\text{LIPS}}, \quad (1.49)$$

$$d^2\Pi_{\text{LIPS}} = \frac{1}{2E'_\chi} \frac{d^3 k'}{(2\pi)^3} \frac{1}{2E'_i} \frac{d^3 p'}{(2\pi)^3} (2\pi)^4 \delta^4(k_\mu + p_\mu - k'_\mu - p'_\mu), \quad (1.50)$$

$$\implies \frac{d\sigma}{d \cos \theta_{\text{cm}}} = \frac{1}{16\pi} \frac{\beta(s)}{2s\beta(s) - \gamma^2(s)} |\bar{\mathcal{M}}|^2, \quad (1.51)$$

where $d^2\Pi_{\text{LIPS}}$ is the 2-body Lorentz invariant phase space.

The advantage of Eq. 1.37 is that it can be used to calculate the capture rate for any interaction given the differential cross-section. The disadvantage is that this computation has to be evaluated numerically, which can be computationally intensive. For this reason, shall now use Eq. 1.48 to derive analytic expressions that will allow us to speed up computations and, in addition, calculate the shape of the interaction rate as a function of the energy loss.

The interaction rate for $d\sigma \propto s^m t^n$ is

$$\begin{aligned} \Gamma^-(E_\chi) = & \sum_{n,m} \frac{(-1)^n \alpha_{n,m}}{128\pi^3 E_\chi k} \int_0^{E_\chi - m_\chi} dq_0 \int \frac{dt_E t_E^n}{(t_E + q_0^2)^{m+\frac{1}{2}}} \\ & \times \sum_{r=0}^m \mathcal{V}_{m,r} \sum_{j=0}^r \binom{r}{j} \varepsilon_{F,i}^{r-j} \frac{(-1)^j q_0^{j+1}}{j+1} h_j \left(\frac{E_i^{t^-} - \varepsilon_{F,i}}{q_0} \right), \end{aligned} \quad (1.52)$$

for elastic scattering with $t_E = -t = q^2 - q_0^2$, where $q_0 = E'_i - E_i$ is the DM energy loss,

$$E_i^{t^-} = - \left(m_n + \frac{q_0}{2} \right) + \sqrt{\left(m_n + \frac{q_0}{2} \right)^2 + \left(\frac{\sqrt{q^2 - q_0^2}}{2} - \frac{m_n q_0}{\sqrt{q^2 - q_0^2}} \right)^2}, \quad (1.53)$$

is the minimum energy of the neutron before the collision, obtained from kinematics, and $h_j(x)$ is a step function with a smooth transition,

$$h_j(x) = \begin{cases} 0, & x > 0 \\ (-x)^{j+1}, & -1 < x < 0 \\ 1, & x < -1 \end{cases}. \quad (1.54)$$

The full derivation of this interaction rate can be found in Appendix A. Our result for Γ^- is an extension of that presented in Ref. [10], where the interaction rate was calculated only in the case of low energy and a constant matrix element. It is valid at all energy ranges. The differential interaction rate $\frac{d\Gamma}{dq_0}(E_\chi, q_0)$ is then just the integrand of Eq. 1.52. We will use $\frac{d\Gamma}{dq_0}$ to obtain normalised shapes for the differential interaction spectrum, while we will use Ω^- when we need the total interaction rate, such as in the capture rate.

Kinematics, and the phase space allowed by $h_j(x)$ in Eq. 1.52, determine the maximum energy that a DM particle can lose in a single scattering interaction, q_0^{MAX} . The details of how to obtain q_0^{MAX} are given in Appendix A.2.1. For DM capture, the value of q_0^{MAX} depends primarily on the DM mass, as is illustrated in the left panel of Fig. 1.2. We can see that for low m_χ , $q_0^{\text{MAX}} \propto m_\chi$, while, for $m_\chi \gg m_n$, it plateaus to values between $q_0^{\text{MAX}} \sim 3 - 6$ GeV. Both q_0^{MAX} and $\frac{d\Gamma}{dq_0}$ also depend on $\varepsilon_{F,n}$ and B . Changing $\varepsilon_{F,n}$ has a very mild effect on the value of q_0^{MAX} (see right panel of Fig. 1.2) and on the shape of the normalised spectrum (see Fig. 1.3). On the other hand, increasing B has the main effect of reducing q_0^{MAX} (see right panel of Fig. 1.2), but only a mild effect on the shape of the profile expressed as a function of the normalised energy loss

$$q_0^{\text{norm}} = \frac{q_0}{q_0^{\text{MAX}}}. \quad (1.55)$$

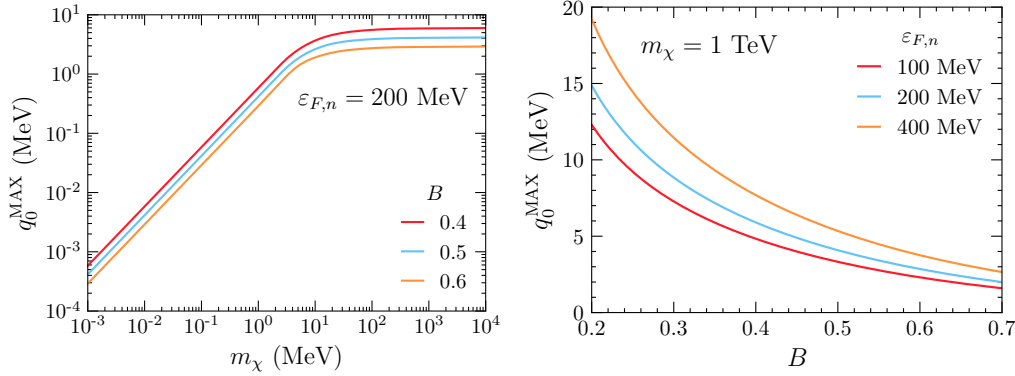


Figure 1.2: Left: q_0^{MAX} vs. m_χ for $\epsilon_{F,n} = 200 \text{ MeV}$ and different values of B . Right: q_0^{MAX} as a function of B for different values of $\epsilon_{F,i}$ and $m_\chi = 1 \text{ TeV}$.

We apply our results for $\frac{d\Gamma}{dq_0}$ to DM-neutron interactions, and in particular those with differential cross-sections that depend only on the transferred momentum $t = (k^\mu - k'^\mu)^2$ and not on the centre of mass energy $s = (p^\mu + k^\mu)^2$.

In Fig. 1.3 we show the normalised differential rates as a function of q_0^{norm} for the four operators D1-D4. The left-hand panels are in the limit $m_\chi \gg m_n$. We can observe that D1 has a softer spectrum, while the D2 and D4 spectra peak towards higher values of q_0 . Varying the chemical potential $\epsilon_{F,n}$ has a very mild effect, shifting the spectrum to lower values of q_0 with increasing values of $\epsilon_{F,n}$. Note that at small values of q_0^{norm} there is a sudden change in the slope of the normalised differential rate, which occurs for all operators but is more evident in D1 (top left panel). This is due to the zero temperature approximation, implicit in Eq. 1.52, where Heaviside functions were used to approximate FD distributions (see Appendix A.2.1); using a finite temperature would produce a smoother spectrum at small q_0^{norm} .

In the right-hand panels of Fig. 1.3, we explore the low DM mass region $m_\chi \ll m_n$. In this case, all operators give rise to similar profiles, the sole difference being that the peak of the profile is now shifted to lower q_0^{norm} for D4 in contrast to D1, with intermediate values for D2 and D3. This is a consequence of Pauli blocking, with this effect depending on the specific power of t that dominates the spectrum. Profiles with lower n ($d\sigma \propto t^n$) peak at higher q_0^{norm} (see Fig. 1.3, right panels). For D4 we have $|\bar{\mathcal{M}}|^2 \propto t^2$, while the matrix elements of D2 and D3 are linear combinations of t and t^2 , and D1 is a combination of all powers of t . Comparing the right panels of Fig. 1.3 with Fig. A.2, we observe that the lowest power of t determines the shape of the final differential interaction rate. Finally, varying $\epsilon_{F,n}$ has a very mild effect, this time shifting the spectrum mostly to higher values of q_0 for higher $\epsilon_{F,n}$.

The fact that the lowest power of t dictates the features of the differential

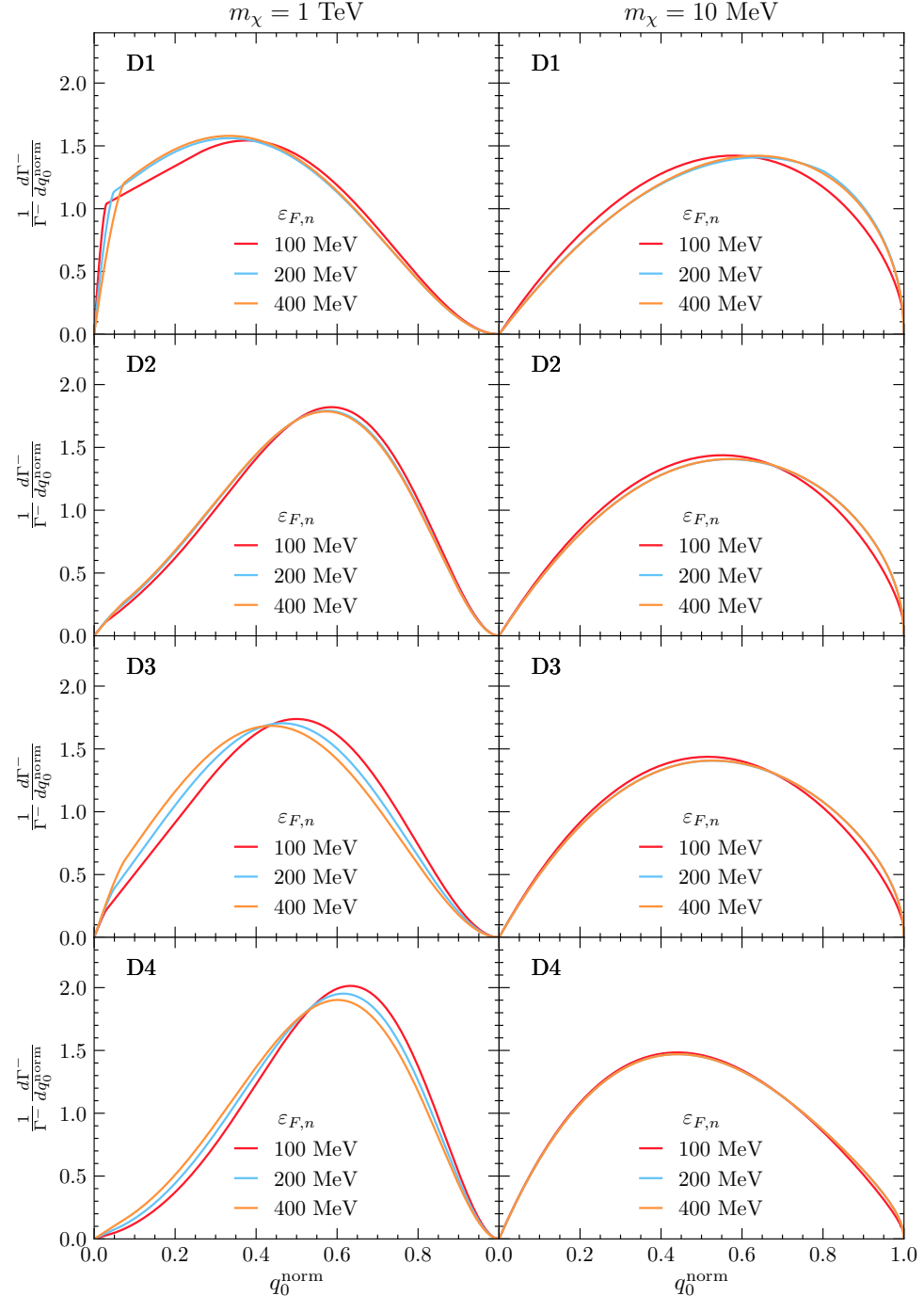


Figure 1.3: Normalised differential interaction rates $\frac{1}{\Gamma} \frac{d\Gamma}{dq_0^{\text{norm}}}$ as a function of q_0^{norm} for different values of $\varepsilon_{F,n}$, $m_\chi = 1 \text{ TeV}$ (left) and $m_\chi = 10 \text{ MeV}$ (right), $B = 0.5$ and operators D1 (first row), D2 (second row), D3 (third row) and D4 (fourth row). Profiles do not depend on m_χ in the limits $m_\chi \gg m_n$ (left) and $m_\chi \ll m_n$ (right).

interaction rate is true also for the interactions that have a dependence on s . As such, by understanding the properties of the interaction rates with $|\bar{\mathcal{M}}|^2 \propto t^n$, we can understand the rates for all the operators in Table. ??.

1.3.1 Pauli Blocking

The DM interaction rate, Eq. 1.48, will be proportional to the number of target particles available to scatter off. Classically, this is the total number of targets within the star. However, the quantum degeneracy of the species within compact objects, due to the extreme densities, leads to a reduction in the number of available initial state target particles the DM can scatter off. To understand this, consider the $T \rightarrow 0$ approximation, in which all initial states with energies $E_i < \varepsilon_{F,i}$ are occupied. These states are known as the “Fermi sea”. In order for the DM to scatter off one of these states, it must impart enough energy to kick the target out of the Fermi sea, such that

$$E'_i = E_i + q_0 > \varepsilon_{F,i}, \quad (1.56)$$

imposing a lower limit on the energy transfer required for an interaction to take place. This effectively reduces the number of available targets to only those with kinetic energies between $\varepsilon_{F,n} - q_0$ and $\varepsilon_{F,i}$. This suppression of the initial state phase space is known as Pauli blocking (PB), and is a completely quantum phenomenon. In this limit, we necessarily have $\Gamma^- \rightarrow 0$ for $q_0 \rightarrow 0$. It is also worth noting that Pauli blocking only affects the interaction rate when $q_0 \leq \varepsilon_{F,n}$.

To assess the impact of PB on the DM differential interaction rate, in Fig. 1.4 we compare the rate with (blue solid lines) and without (light blue dashed lines) Pauli blocking, for $B = 0.5$ and constant DM-neutron cross-section. When Pauli blocking can be neglected, the interaction rate is obtained straightforwardly from Eq. 1.48 by stripping away the $(1 - f_{FD}(E'_i))$ factor. The difference between the computations is shaded in light blue. In the top left panel, we see that the rate begins to be suppressed from PB at $q_0 \sim \varepsilon_{F,i} = 100$ MeV for a 1 GeV DM. In the top right plot, we increase the neutron chemical potential from $\varepsilon_{F,n} = 100$ MeV to $\varepsilon_{F,n} = 400$ MeV. Given that in this case $q_0^{\text{MAX}} \sim 0.4m_\chi \sim 400$ MeV, almost the whole energy range is affected by PB. The higher $\varepsilon_{F,n}$ changes the spectra (both with and without PB) such that the unsuppressed rate is no longer flat at low q_0 . The PB suppressed rate reaches a maximum at values of q_0 slightly below q_0^{MAX} , and then decreases towards 0 at lower q_0 . In the middle panels, $m_\chi = 100$ MeV, and $q_0^{\text{MAX}} \sim 40$ MeV $\ll \varepsilon_{F,n}$. In this case, it is evident that PB affects the spectrum over the full $q_0 = q_0^{\text{MAX}}$ range. In the bottom row, we set $m_\chi = 10$ MeV. As expected, for lighter DM, the effects of PB are even more pronounced.

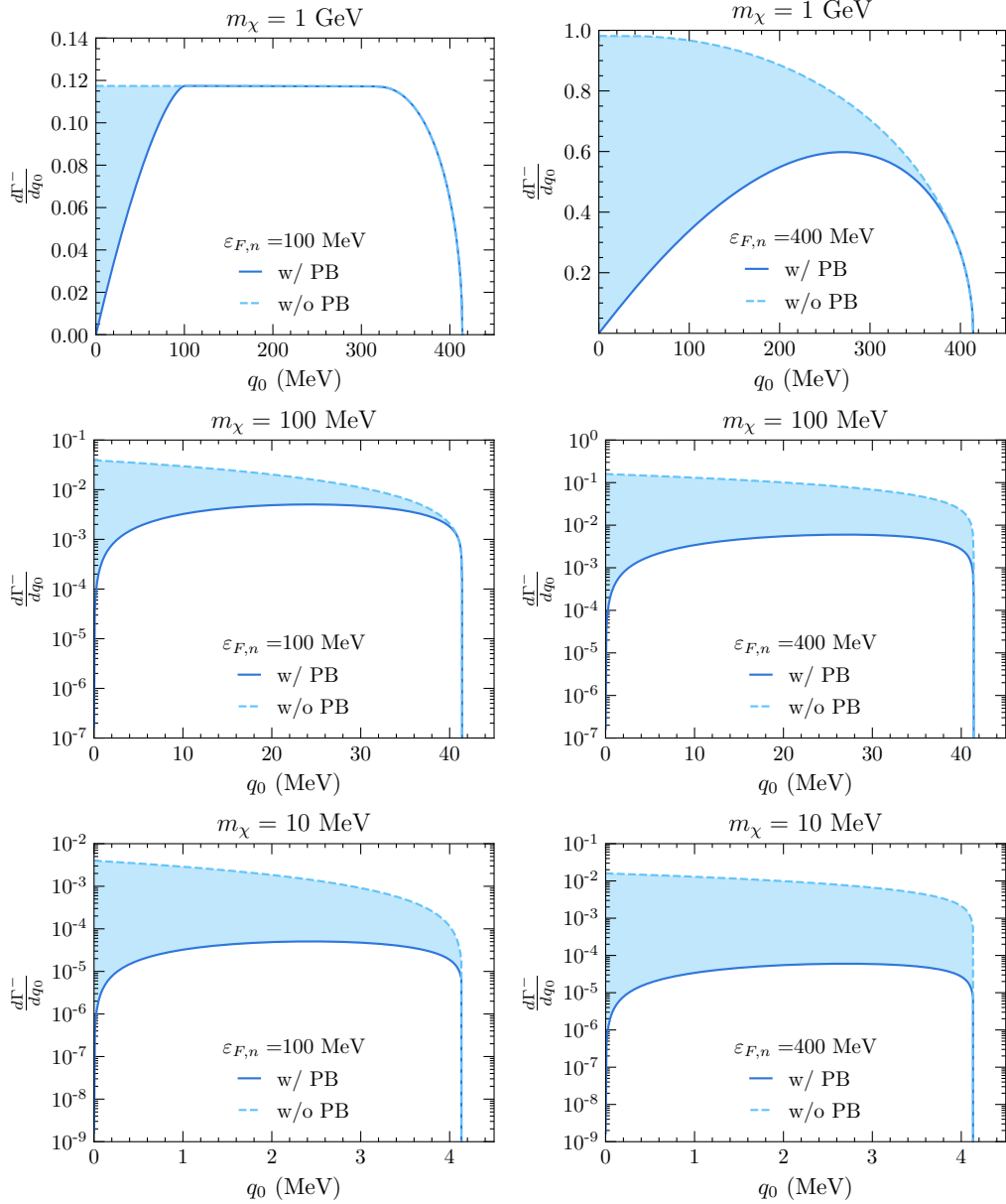


Figure 1.4: Differential interaction rates $\frac{d\Gamma}{dq_0}$ as a function of the energy loss q_0 for different values of m_χ and $\varepsilon_{F,n}$, constant cross-section and $B = 0.5$. Blue lines refer to the result that includes Pauli blocking, while the light blue dashed lines refer to the result without PB. Left column: $\varepsilon_{F,n} = 100$ MeV, right column: $\varepsilon_{F,n} = 400$ MeV. Top: $m_\chi = 1$ GeV, middle: $m_\chi = 100$ MeV, bottom: $m_\chi = 10$ MeV.

To understand how the effect of PB varies throughout the star, we can analyse the radial profiles of the capture rates dC/dr . In Fig. 1.5 we plot the differential capture rate as a function of the NS radius, with and without Pauli blocking. We see that Pauli blocking is most significant at low DM mass, below about 1 GeV, and becomes insignificant for higher masses. Pauli blocking has a larger impact on the differential capture rate deeper into the NS interior and has a negligible effect at the surface. This is particularly apparent in the top left panel of Fig. 1.5. This is because the chemical potential is higher in the NS interior than it is near the crust, as seen in the radial $\varepsilon_{F,i}$ profile in the bottom left panel of Fig. ??.

1.4 Capture in the Low, Intermediate and High Mass Regimes

Having assembled all the required machinery, we are ready to explore the properties of the capture rate in the three mass regimes outlined in Eq. 1.26. Given the computational load required to evaluate Eq. 1.24 in general, we aim to provide approximations that are numerically more efficient where possible. We also discuss the high DM mass regime where multiple scatterings are required for capture, and how this is affected by Pauli blocking.

1.4.1 Low and intermediate DM mass range

In sections 1.2 and 1.3, we have derived general expressions to numerically calculate the DM capture and interaction rates, Eqs. 1.24 and 1.37 respectively. Using these expressions, we can write the complete expression for the capture rate as a function of the differential DM-neutron cross-section

$$C = \frac{2\rho_\chi}{\pi v_* m_\chi^2} \text{Erf} \left(\sqrt{\frac{3}{2}} \frac{v_*}{v_d} \right) \int_0^{R_*} dr \frac{r^2 \zeta(r)}{\sqrt{B(r)}} \int dt dE_i ds \frac{d\sigma}{d \cos \theta_{\text{cm}}} \frac{E_i s}{\beta(s) \gamma(s)} (1.57) \\ \times f_{\text{FD}}(E_i, r) (1 - f_{\text{FD}}(E'_i, r)),$$

where the functions β and γ were given in section 1.2.3. Recall that in the limit $T \rightarrow 0$, $f_{\text{FD}}(E_i, r)$ and $1 - f_{\text{FD}}(E'_i, r)$ reduce to the step functions, $\Theta(\varepsilon_{F,i}(r) - E_i)$ and $\Theta(E'_i - \varepsilon_{F,i}(r))$, respectively.

Exchanging the differential cross-section for the squared matrix allows for easier

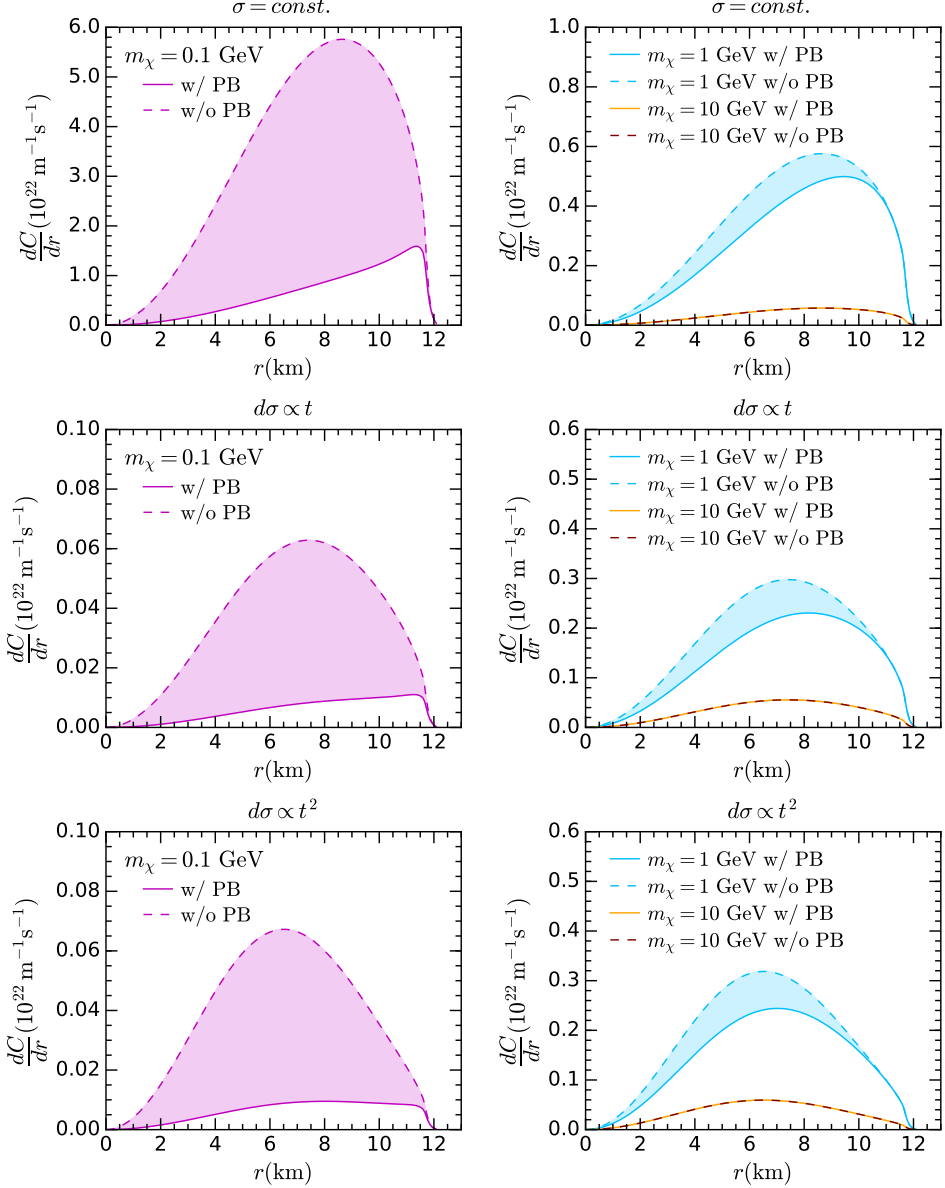


Figure 1.5: Differential capture rate as a function of the NS radius r , with (solid) and without (dashed) Pauli blocking, for the EoS benchmark BSk24-2. Top: constant cross-section, center: $d\sigma \propto t$, bottom: $d\sigma \propto t^2$.

examination of the operators in Table ??, and so we write the capture rate as

$$C = \frac{\rho_\chi}{8\pi^2 v_\star m_\chi^2} \text{Erf} \left(\sqrt{\frac{3}{2}} \frac{v_\star}{v_d} \right) \int_0^{R_\star} dr \frac{r^2 \zeta(r)}{\sqrt{B(r)}} \int dt dE_i ds \frac{|\bar{M}|^2 E_i}{2s\beta(s) - \gamma^2(s)} \frac{s}{\gamma(s)} (1.58)$$

$$\times f_{\text{FD}}(E_i, r)(1 - f_{\text{FD}}(E'_i, r)).$$

This expression can be used to numerically calculate the single scatter capture rate of DM in compact objects, in the optically thin regime. In general, this must be used for low-mass DM where PB is in effect.

As discussed in section 1.3.1, PB eventually becomes negligible for DM with masses $\gtrsim \mu_{F,i}$. Hence, between this mass and the point where multiple scattering becomes important, PB can be neglected and a simplified capture rate be obtained. For nucleon targets, this range is between $1 \text{ GeV} \lesssim m_\chi \lesssim 10^6 \text{ GeV}$, which we call the intermediate mass range.

The resulting simplified capture rate differs slightly depending on whether the matrix element depends only on t , or if it has explicit s dependence. We present the full derivations of these results in Appendix **ADD APPENDICIES** First, for $|\bar{M}|^2 = at^n$, the previous expression can be simplified to

$$C \sim C_{\text{approx}} = \frac{4\pi}{v_\star} \frac{\rho_\chi}{m_\chi} \text{Erf} \left(\sqrt{\frac{3}{2}} \frac{v_\star}{v_d} \right) \int_0^{R_\star} r^2 dr n_i(r) \frac{1 - B(r)}{B(r)} \langle \sigma(r) \rangle, \quad (1.59)$$

$$\langle \sigma(r) \rangle = \left\langle \int dt \frac{d\sigma}{dt} \right\rangle_s = \frac{a}{16\pi m_\chi^2} \frac{1}{n+1} \left(\frac{4(1 - B(r))m_\chi^2}{B(r)(1 + \mu^2)} \right)^n. \quad (1.60)$$

For s -dependent matrix elements the result is very similar, with the only difference being that the cross-section is not averaged over s , and instead s is fixed to a particular value as detailed in Appendix **ADD APPENDIX**. Writing the matrix element as $|\bar{M}|^2 \propto \bar{g}(s)t^n$, for with g some function of s , we arrive at the result

$$C \sim C_{\text{approx},s} = \frac{4\pi}{v_\star} \frac{\rho_\chi}{m_\chi} \text{Erf} \left(\sqrt{\frac{3}{2}} \frac{v_\star}{v_d} \right) \int_0^{R_\star} r^2 dr n_i(r) \frac{1 - B(r)}{B(r)} \sigma(r), \quad (1.61)$$

$$\sigma(r) = \int dt \frac{d\sigma}{dt} = \frac{1}{16\pi \left(m_i^2 m_\chi^2 + 2m_i m_\chi / \sqrt{B(r)} \right)} \frac{\bar{g}(s_0)}{(n+1)} \times \left[\frac{4(1 - B(r))m_\chi^2}{B(r)(1 + \mu^2) + 2\sqrt{B(r)}\mu} \right]^n, \quad (1.62)$$

$$s_0 = m_i^2 + m_\chi^2 + 2 \frac{E_i m_\chi}{\sqrt{B(r)}}. \quad (1.63)$$

As with the differential interaction rates, it is the t -dependence of the matrix elements that dictate the key features of the capture rate.

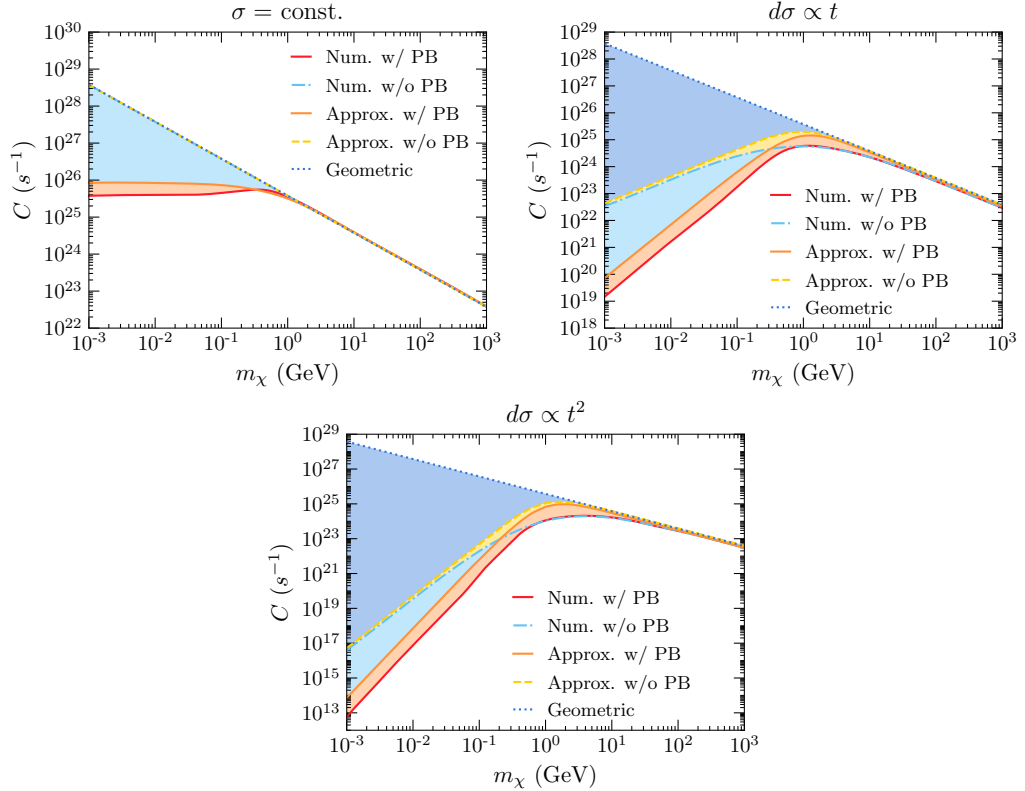


Figure 1.6: Capture rate as a function of the DM mass with cross-sections normalised to $\sigma = \sigma_{\text{ref}} \sim 1.7 \times 10^{-45} \text{ cm}^2$, for EoS BSk24-2, calculated with and without Pauli blocking. Top left: constant cross-section. Top right: $d\sigma \propto t$, bottom: $d\sigma \propto t^2$, where t is the Mandelstam variable. All rates are normalised to the geometric limit at large DM mass.

In Fig. 1.6, we show the capture rate as a function of the DM mass for matrix elements proportional to t^n , for $n = 0, 1, 2$ and the NS benchmark model BSk24-2. Numerical results obtained using Eq. 1.58 are shown in solid red; results using the same equation but removing the theta function that enforces Pauli blocking are depicted in light blue; and the approximation for intermediate DM masses, Eq. 1.59, in yellow. We show the geometric limit, Eq. 1.25, in blue for comparison. The capture rates were all normalised to the geometric limit at large DM mass where PB is negligible. In the same plots, we also show in brown the result obtained from using a modified version of Eq. 1.59 to include Pauli blocking. This is achieved by including the ratio between the differential the interaction rate, Γ^- , calculated with and without Pauli blocking. This comparison was done in section 1.3.1 for various values of B and $\varepsilon_{F,n}$.

From Fig. 1.6, we can see that Eq. 1.59 is indeed a good approximation to the numerical results obtained without Pauli blocking, and can be safely used for DM masses from a few GeV up to $m_\chi \sim 10^6$ GeV, where multiple scattering becomes relevant. On the other hand, for $m_\chi \lesssim 100$ MeV the brown line is no longer a good approximation to the numerical result with Pauli blocking, as it always overestimates the capture rate by nearly an order of magnitude. Therefore, to accurately account for the effects of PB for low mass DM, the complete expression for the capture rate, Eq. 1.58 must be used and evaluated numerically.

We now compare our full numerical capture rate calculation, Eq. 1.58, with that of Ref. [8], in Fig. 1.7. The capture rates calculated in Ref. [8] correctly include the stellar structure and Pauli blocking, however, they do not account for general relativistic corrections, and the authors only considered the case of a constant cross-section, $\sigma = 10^{-45} \text{ cm}^2$. To make the comparison as fair as possible, we have selected NS configurations that match those of Figs. 1 and 14 of Ref. [8], namely their Model A (BSk20-1): $M_\star \simeq 1.52 M_\odot$, $R_\star \simeq 11.6$ km and Model D (BSk21-2): $M_\star \simeq 2.11 M_\odot$ and $R_\star \simeq 12.0$ km. We denote these new benchmark models as BSk26-1 (left panel of Fig. 1.7) and BSk24-5 (right panel). Note that we were not able to use the BSk20 and BSk21 functionals, since there are no publicly available fits for the chemical potentials and particle abundances for those EoS families. However, as discussed earlier in section ??, BSk26 (BSk24) yields configurations that are almost indistinguishable from those obtained with BSk20 (BSk21) [11].

We can see in the left panel of Fig. 1.7 that in the non-Pauli suppressed region, $m_\chi \gtrsim 1$ GeV, our capture rate calculation in the optical thin limit (solid magenta) exceeds that of Ref. [8] (dot-dashed blue) by a factor of ~ 4 . When Pauli blocking is active, our capture rate calculation is about one order of magnitude higher than the classical calculation. Recall that Ref. [8] accounts for neither gravitational focusing nor relativistic kinematics. We also show in dashed light blue the approximation given in Ref. [12], which accounts for Pauli blocking with a suppression factor that depends on the neutron Fermi momentum $\sim m_\chi v_{esc}/p_{F,n}$ for $m_\chi < m_n$. Though

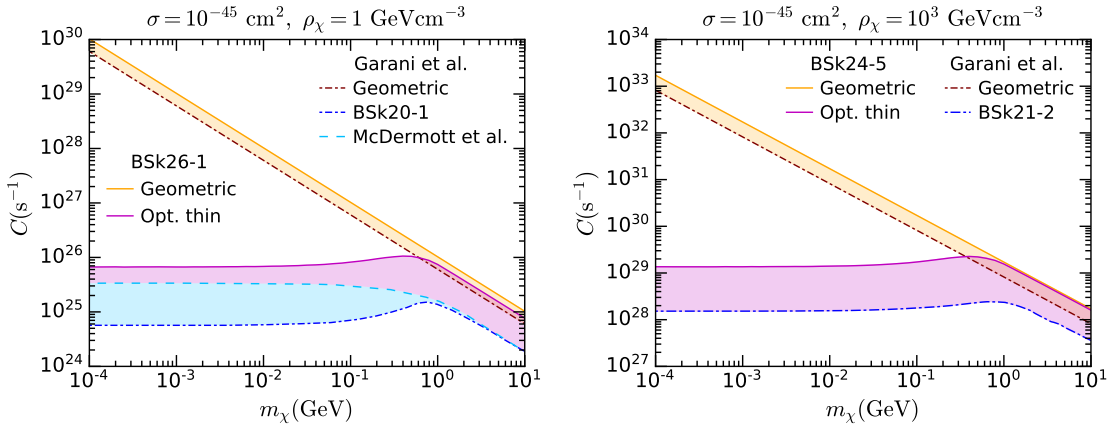


Figure 1.7: Left: Capture rate in the optically thin (magenta) and geometric (orange) limits as a function of the DM mass for constant cross-section $\sigma = 10^{-45} \text{ cm}^2$, $\rho_\chi = 1 \text{ GeV cm}^{-3}$ and BSk26 functional for $M_\star \simeq 1.52M_\odot$ and $R_\star \simeq 11.6 \text{ km}$ denoted as BSk26-1. Capture rate calculations from Ref. [8] for a NS configuration with EoS BSk20-1 [13] equivalent to BSk26-1, are shown for comparison. Right: Same as left but for $\rho_\chi = 10^3 \text{ GeV cm}^{-3}$ and the benchmark model BSk24-5 equivalent to BSk21-2 in Ref. [8]: $M_\star \simeq 2.11M_\odot$ and $R_\star \simeq 12.0 \text{ km}$.

this approximation fails to reproduce the capture rate shape due to Pauli blocking in the DM mass range $[0.1 \text{ GeV}, 10 \text{ GeV}]$, it underestimates the capture rate by only a factor of 2 when the DM mass is below 0.1 GeV. Finally, we compare the geometric limit of Eq. 1.25 (solid orange) that incorporates GR effects [6] with the non-relativistic expression in Ref. [8] (dot-dashed brown). We observe that the former is $\sim 67\%$ greater than the latter, mostly due to the $1/B(R_\star)$ GR correction [5, 7]. Similar conclusions are obtained when comparing capture rate calculations for Model D of Ref. [8] (their Fig. 14) with our approach, as illustrated in the right panel of Fig. 1.7.

1.4.2 Multiple Scattering

The capture rate expressions obtained in the previous section assume that the cross-section is small enough that the star is in the “optically thin” regime, and that a single scatter is sufficient to capture the DM. These assumptions break down if the DM-target cross-section is $\gtrsim \mathcal{O}(\sigma_{\text{th}})$, or if the DM mass exceeds $m_\chi \sim 10^6 \text{ GeV}$, respectively. In this section, we focus on addressing the latter concern, relegating the discussion on the NS opacity in Appendix ?? as it is not required for the remainder of this work. To that end, we now explain how to modify our previous

capture rate expressions to account for multiple scattering in a degenerate media⁴

In deriving Eq. 1.57 we had assumed that the DM velocity at infinity, u_χ , can be neglected, such that any interaction where the DM loses energy resulted in its capture. If we instead keep the leading order u_χ contribution to the total DM energy, the DM energy at infinity is instead

$$E_\chi^\infty \sim m_\chi \left(1 + \frac{1}{2} u_\chi^2\right), \quad (1.64)$$

and at a distance r from the star it gets boosted to

$$E_\chi(r) = \frac{m_\chi}{\sqrt{B(r)}} \left(1 + \frac{1}{2} u_\chi^2\right). \quad (1.65)$$

Therefore, the amount of energy that must be lost in order for the DM to be captured is

$$E_\chi^C(r) = \frac{1}{2} u_\chi^2 \frac{m_\chi}{\sqrt{B(r)}}. \quad (1.66)$$

$$\sim 6 \times 10^{-7} \text{ GeV} \left(\frac{u_\chi}{270 \text{ km s}^{-1}}\right)^2 \left(\frac{m_\chi}{1 \text{ GeV}}\right) \left(\frac{0.5}{B(r)}\right)^{1/2}, \quad (1.67)$$

For DM masses $m_\chi \gtrsim 10^6 \text{ GeV}$ that scatters on nucleon targets, the capture probability is smaller than 1 and becomes tiny as we increase the DM mass to large values. To account for this effect, we proceed in the following way. First, instead of setting the DM speed at infinity to 0, as we did in the previous section, we now assume that the DM particles have a speed $u_\chi \ll 1$ that follows a Maxwell-Boltzmann (MB) distribution, Eq. ???. The probability density function of the energy lost by a DM particle is

$$\xi(q_0, E_\chi, \mu_{F,n}) = \frac{1}{\Gamma(E_\chi)} \frac{d\Gamma}{dq_0}(q_0, E_\chi, \mu_{F,n}), \quad (1.68)$$

where $\frac{d\Gamma}{dq_0}$ is the DM differential interaction rate, calculated in Appendix ???. The function ξ is defined for any $q_0 \geq 0$, however, due to kinematics, the function is non-zero only for $q_0 \leq q_0^{\text{MAX}}$. ξ depends on $B(r)$ through the ratio E_χ/m_χ , and for brevity we will simply write $\xi(q_0)$.

We can define the probability to lose an amount of energy of at least δq_0 in a single collision as

$$P_1(\delta q_0) = \int_{\delta q_0}^{\infty} dx \xi(x). \quad (1.69)$$

⁴For a recent discussion on multiple scattering within non-relativistic stars, or with ions in WDs, see Ref. [14].

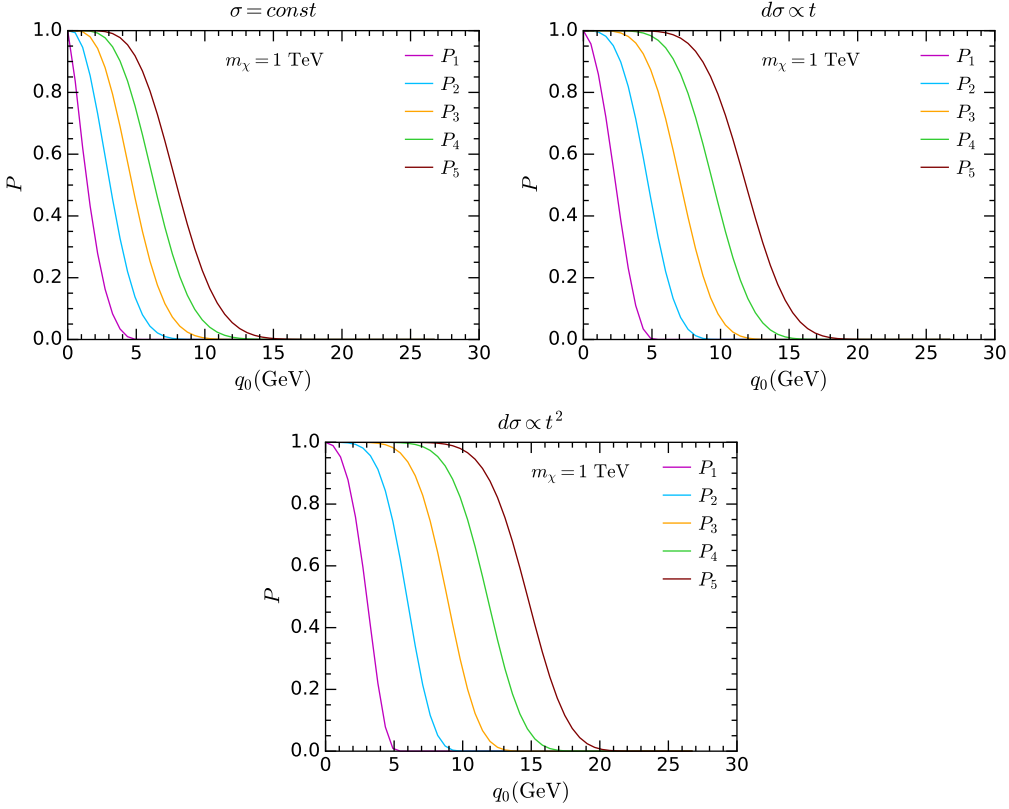


Figure 1.8: Probabilities to lose an energy δq_0 after 1, ..., 5 scatterings, P_1, \dots, P_5 , as a function of the energy loss q_0 , assuming $B = 0.5$ and $\mu_{F,n} = 400 \text{ MeV}$. Results are shown for different dependence on the cross-section on the Mandelstam variable t : constant DM-neutron cross-section (top left), $d\sigma \propto t$ (top right) and $d\sigma \propto t^2$ (bottom).

In the same way, the probability to lose at least the same amount of energy after 2 collisions is

$$P_2(\delta q_0) = P_1(\delta q_0) + \int_{\delta q_0}^{\infty} dy \int_0^y dx \xi(x) \xi(y-x) = P_1(\delta q_0) + \int_0^{\delta q_0} dz P_1(\delta q_0 - z) \xi(z)$$

Thus, we obtain the following recursive relation for P_N ,

$$P_{N+1}(\delta q_0) = P_N(\delta q_0) + \int_0^{\delta q_0} dz P_N(\delta q_0 - z) \xi(z). \quad (1.71)$$

Fig. 1.8 shows how the probability functions P_1, \dots, P_5 depend on the Mandelstam variable t through the differential cross-section. We show results for $\sigma = \text{const}$. (top left), $d\sigma \propto t$ (top right) and $d\sigma \propto t^2$ (bottom), with the values $B = 0.5$, $\mu_{F,n} = 400 \text{ MeV}$.

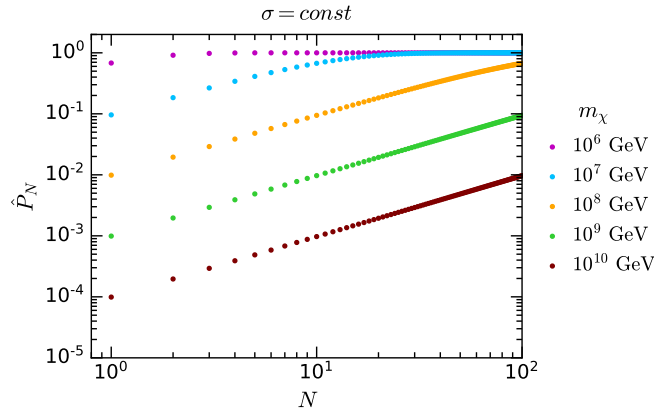


Figure 1.9: Cumulative probability \hat{P}_N for $B = 0.5$, $\mu_{F,n} = 400$ MeV for constant $|\bar{M}|^2$ as a function of the number of scatterings N for several DM masses.

We define the probability of a DM particle to be captured after exactly N scatterings by averaging over the MB energy distribution

$$c_N(r) = \frac{1}{\int_0^\infty \frac{f_{\text{MB}}(u_\chi)}{u_\chi} du_\chi} \int_0^\infty \frac{f_{\text{MB}}(u_\chi)}{u_\chi} du_\chi \left[P_N \left(\frac{1}{2} \frac{m_\chi u_\chi^2}{\sqrt{B(r)}} \right) - P_{N-1} \left(\frac{1}{2} \frac{m_\chi u_\chi^2}{\sqrt{B(r)}} \right) \right]$$

where c_N depends on r through the dependence of P_1 on $B(r)$. Note that although our results will assume a Maxwell-Boltzmann velocity distribution, it is straightforward to repeat the calculations with any other DM velocity distribution. The cumulative probability \hat{P}_N that a DM particle is captured after N interactions with a total energy loss $\delta q_0 = E_\chi^C$ is

$$\hat{P}_N(r) = \sum_{i=1}^N c_i = \frac{1}{\int_0^\infty \frac{f_{\text{MB}}(u_\chi)}{u_\chi} du_\chi} \int_0^\infty \frac{f_{\text{MB}}(u_\chi)}{u_\chi} du_\chi P_N \left(\frac{1}{2} \frac{m_\chi}{\sqrt{B(r)}} u_\chi^2 \right). \quad (1.73)$$

The resulting cumulative probability is shown as a function of the number of scatterings N in Fig. 1.9, for constant cross-section and several DM masses. The cumulative probability \hat{P}_N for the above values of $B, \mu_{F,n}$ is well approximated by the function

$$\hat{P}_N \sim 1 - e^{-\frac{Nm^*}{m_\chi}}. \quad (1.74)$$

In particular, for single scattering

$$c_1 = \hat{P}_1 \sim 1 - e^{-\frac{m^*}{m_\chi}}. \quad (1.75)$$

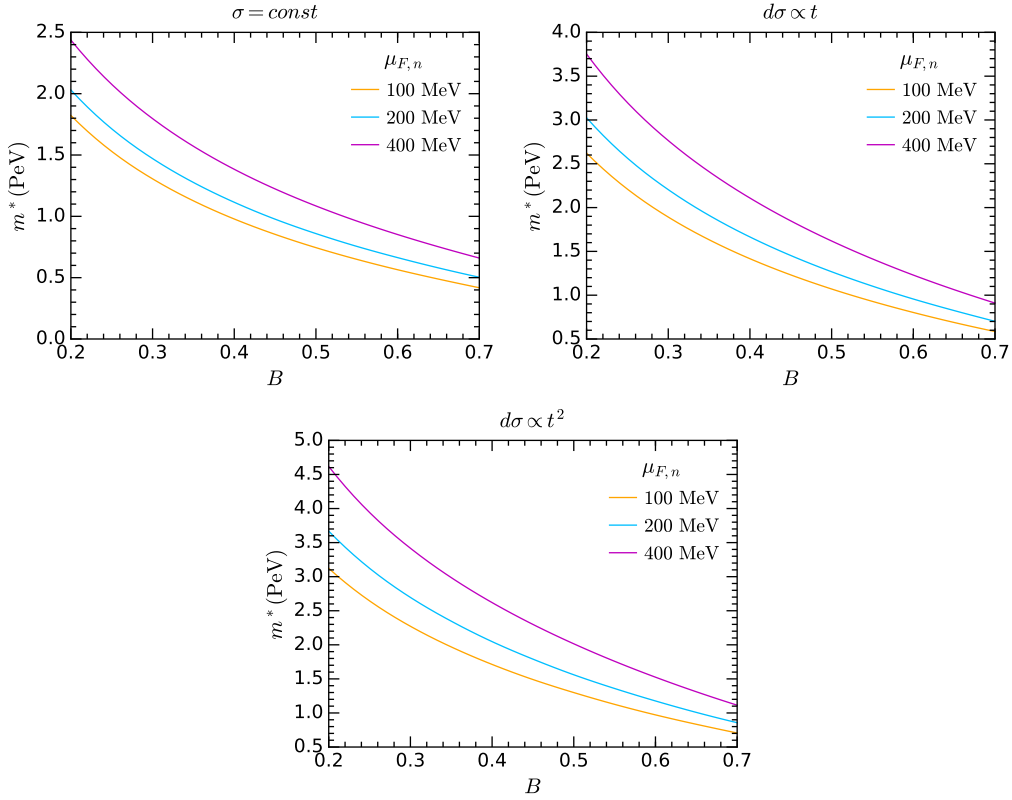


Figure 1.10: Value of m^* as a function of B for different values of $\mu_{F,n}$, $\sigma = \text{const.}$ (top left), $d\sigma \propto t$ (top right) and $d\sigma \propto t^2$ (bottom).

Further discussion of the multi-scattering regime, and justification of this fitting function, can be found in Appendix ???. For the values $B = 0.5$ and $\mu_{F,n} = 400$ MeV, we find

$$m^* = 1.08 \times 10^6 \text{ GeV}, \quad |\bar{M}|^2 \propto t^0, \quad (1.76)$$

$$m^* = 1.62 \times 10^6 \text{ GeV}, \quad |\bar{M}|^2 \propto t^1, \quad (1.77)$$

$$m^* = 2.01 \times 10^6 \text{ GeV}, \quad |\bar{M}|^2 \propto t^2. \quad (1.78)$$

We illustrate how m^* varies with B and $\mu_{F,n}$ in Fig. 1.10.

A

Derivation of Dark Matter Interaction Rates in Degenerate Media

A.1 General Interaction Rates

The most general form of the interaction rate, following Ref. [10], can be written as

$$\Gamma = \int \frac{d^3 k'}{(2\pi)^3} \frac{1}{(2E_\chi)(2E'_\chi)(2m_i)(2m_i)} \Theta(E'_\chi - m_\chi) \Theta(\pm q_0) S(q_0, q), \quad (\text{A.1})$$

$$S(q_0, q) = 2 \int \frac{d^3 p}{(2\pi)^3} \int \frac{d^3 p'}{(2\pi)^3} \frac{m_i^2}{E_i E'_i} |\bar{\mathcal{M}}|^2 (2\pi)^4 \delta^4(k_\mu + p_\mu - k'_\mu - p'_\mu) \\ \times f_{\text{FD}}(E_i)(1 - f_{\text{FD}}(E'_i)) \Theta(E_i - m_i) \Theta(E'_i - m_i), \quad (\text{A.2})$$

The δ -function can be used to perform the $d^3 p'$ integrations, leaving

$$S(q_0, q) = \frac{1}{2\pi^2} \int d^3 p \frac{m_i^2}{E_i E'_i} |\bar{\mathcal{M}}|^2 \delta(q_0 + E_i - E'_i) f_{\text{FD}}(E_i)(1 - f_{\text{FD}}(E'_i)) \\ \times \Theta(E_i - m_i) \Theta(E'_i - m_i). \quad (\text{A.3})$$

After this, the final state target energy is fixed to

$$E'_i(E_i, q, \theta) = \sqrt{m_i^2 + (\vec{p} + \vec{q})^2} \quad (\text{A.4})$$

$$= \sqrt{E_i^2 + q^2 + 2qp \cos \theta} > m_i, \quad \forall p, q, \theta, |\cos \theta| < 1, \quad (\text{A.5})$$

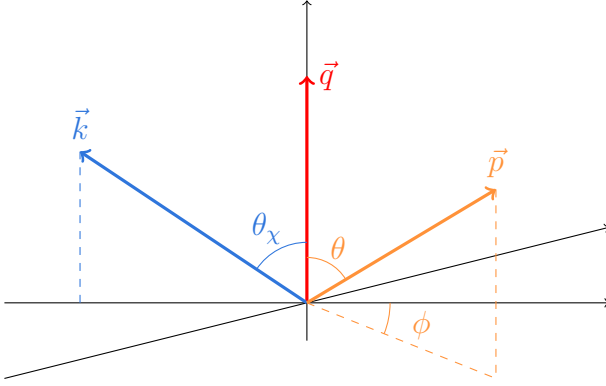


Figure A.1: Schematic of kinematics for dark matter interacting with a target in the frame of the star. We set the momentum transfer to lie along the z -axis with the initial momenta defined relative to it.

where θ is the angle between the target initial momentum and the transferred momentum, \vec{q} , that is defined below. To perform the remaining integrals, we write $d^3p = pE_idE_i d\cos\theta d\phi$. The kinematics of this interaction are depicted in Fig. A.1, where the incoming momenta are defined relative to the momentum transfer that is set to lie along the z -axis. In doing so, we must account for the fact that in this frame we cannot assume all three of the vectors are coplanar, and assign the additional azimuthal angle ϕ to the target momentum.

In general, the squared matrix elements we are interested in can be expressed as polynomials in the Mandelstam variables s and t , such that

$$|\bar{\mathcal{M}}|^2 = \sum_{n,m} \alpha_{n,m} t^n s^m. \quad (\text{A.6})$$

Writing $s = m_\chi^2 + m_i^2 + 2E_\chi E_i - 2\vec{p} \cdot \vec{k}$, the quantity $\vec{k} \cdot \vec{p}$ is obtained by analysing the kinematics of the interaction. From the diagram in Fig. A.1, we can write the initial momenta as

$$\vec{k} = (k \sin \theta_\chi, 0, k \cos \theta_\chi), \quad (\text{A.7})$$

$$\vec{p} = (p \sin \theta \cos \phi, p \sin \theta \sin \phi, p \cos \theta). \quad (\text{A.8})$$

The angles can then be expressed in terms of the other kinematic quantities by

noting that

$$E'_\chi = \sqrt{m_\chi^2 + (\vec{k} - \vec{q})}, \quad (\text{A.9})$$

$$\implies (E_\chi - q_0)^2 = m_\chi^2 + (k^2 + q^2 - 2kq \cos \theta_\chi) \quad (\text{A.10})$$

$$\implies \cos \theta_\chi = \frac{q^2 - q_0^2 + 2E_\chi q_0}{2q \sqrt{E_\chi^2 - m_\chi^2}}, \quad (\text{A.11})$$

$$E'_i = \sqrt{m_i^2 + (\vec{p} + \vec{q})}, \quad (\text{A.12})$$

$$(\text{A.13})$$

for the dark matter angle, and

$$\implies (E_i + q_0)^2 = m_i^2 + (p^2 + q^2 + 2pq \cos \theta) \quad (\text{A.14})$$

$$\implies \cos \theta = \frac{q_0^2 - q^2 + 2E_i q_0}{2q \sqrt{E_i^2 - m_i^2}} \quad (\text{A.15})$$

for the target angle. These result in

$$\vec{k} \cdot \vec{p} = kp \sin \theta_\chi \sin \theta \cos \phi + kp \cos \theta_\chi \cos \theta \quad (\text{A.16})$$

$$\begin{aligned} &= kp \left[\sqrt{1 - \frac{(q^2 - q_0^2 + 2E_\chi q_0)^2}{4q^2(E_\chi^2 - m_\chi^2)}} \sqrt{1 - \frac{(q_0^2 - q^2 + 2E_i q_0)^2}{4q^2(E_i^2 - m_i^2)}} \cos \phi \right. \\ &\quad \left. + \frac{(q^2 - q_0^2 + 2E_\chi q_0)(q_0^2 - q^2 + 2E_i q_0)}{4q^2 \sqrt{E_\chi^2 - m_\chi^2} \sqrt{E_i^2 - m_i^2}} \right] \end{aligned} \quad (\text{A.17})$$

$$\begin{aligned} &= \frac{(q^2 - q_0^2 + 2E_\chi q_0)(q_0^2 - q^2 + 2E_i q_0)}{4q^2} \\ &\quad + \sqrt{E_\chi^2 - m_\chi^2 - \frac{(q^2 - q_0^2 + 2E_\chi q_0)^2}{4q^2}} \sqrt{E_i^2 - m_i^2 - \frac{(q_0^2 - q^2 + 2E_i q_0)^2}{4q^2}} \cos \phi. \end{aligned} \quad (\text{A.18})$$

This makes explicit that s is now a function of the azimuthal angle ϕ .

We then use the remaining delta function to integrate over θ , giving rise to a step function $\Theta(1 - \cos^2 \theta(q, q_0, E_i))$, leaving the

$$S(q_0, q) = \alpha t^n \frac{m_i^2}{2\pi^2 q} \int dE_i d\phi s^m f_{\text{FD}}(E_i) (1 - f_{\text{FD}}(E_i + q_0)) \Theta(E_i) \Theta(1 - \cos^2 \theta). \quad (\text{A.19})$$

It will be more convenient to work with the kinetic energies of the targets rather than their total energies, as we are only interested in elastic scattering. From here on out, E_i will refer to the kinetic energy of the target, i.e. $E_i \rightarrow E_i + m_i$.

This is compensated by using the Fermi kinetic energy in the FD distributions, $\varepsilon_{F,i} = \mu_{F,i} - m_i$.

The ϕ integrals can be easily computed for a given power of s , in general resulting in a messy function of the kinematic variables. However, we know that they will always be a polynomial of degree m , and so to make this explicit while keeping things as tidy as possible, we define the polynomials $\mathcal{U}_m(q^2, q_0, E_\chi, E_i)$ as

$$\mathcal{U}_m = \frac{q^{2m}}{2\pi} \int_0^{2\pi} d\phi s^m = \sum_r \mathcal{V}_{m,r} E_i^r \quad (\text{A.20})$$

where the coefficients of the polynomial, $\mathcal{V}_{m,r}$, are functions of q^2, q_0 , and E_χ . The response function is then

$$S(q_0, q) = \alpha t^n \frac{m_i^2}{\pi q} \int dE_i f_{\text{FD}}(E_i) (1 - f_{\text{FD}}(E_i + q_0)) \frac{\mathcal{U}_m}{q^{2m}} \Theta(E_i) \Theta(1 - \cos^2 \theta). \quad (\text{A.21})$$

Therefore, the integrals we are interested in computing are over the FD distributions, which we call

$$\mathcal{F}_r(E_i, q_0) = \int dE_i E_i^r f_{\text{FD}}(E_i) (1 - f_{\text{FD}}(E_i + q_0)). \quad (\text{A.22})$$

To proceed, make the change to the dimensionless variables

$$x = \frac{E_i - \varepsilon_{F,i}}{T_\star}, \quad z = \frac{q_0}{T_\star}, \quad (\text{A.23})$$

which we can use to write

$$\mathcal{F}_r(E_i, q_0) = T_\star \int dx (\varepsilon_{F,i} + T_\star x)^r f_{\text{FD}}(x) f_{\text{FD}}(-x - z) \quad (\text{A.24})$$

$$= T_\star \int dx \sum_{j=0}^r \binom{r}{j} T_\star^j x^j \varepsilon_{F,i}^{r-j} f_{\text{FD}}(x) f_{\text{FD}}(-x - z) \quad (\text{A.25})$$

$$= \sum_{j=0}^r T_\star^{j+1} \binom{r}{j} \varepsilon_{F,i}^{r-j} \int dx x^j f_{\text{FD}}(x) f_{\text{FD}}(-x - z) \quad (\text{A.26})$$

$$= \sum_{j=0}^r \binom{r}{j} \varepsilon_{F,i}^{r-j} \int dE_i (E_i - \varepsilon_{F,i})^j f_{\text{FD}}(E_i) f_{\text{FD}}(-E_i - q_0) \quad (\text{A.27})$$

$$= \sum_{j=0}^r \binom{r}{j} \varepsilon_{F,i}^{r-j} (-1)^j \frac{q_0^{j+1}}{j+1} g_j \left(\frac{E_i - \varepsilon_{F,i}}{q_0} \right), \quad \text{for } T_\star \rightarrow 0, \quad (\text{A.28})$$

where the final line holds in the zero-temperature approximation in which the FD distributions become Θ -functions, allowing the integrals to be expressed in terms of the function

$$g_j(x) = \begin{cases} 1, & x > 0 \\ 1 - (-x)^{j+1}, & -1 < x < 0 \\ 0, & x < -1 \end{cases} \quad (\text{A.29})$$

The integration range for E_i is obtained from the two Θ -functions. There are two cases to be considered, $t < 0$ and $t > 0$. In the former case, the range become $E_i^{t^-} < E_i < \infty$ and for the latter $0 < E_i < E_i^{t^+}$. These integration bounds are obtained from Eq. A.15, by settting $\cos \theta = 1$, and are given by

$$E_i^{t^-} = -\left(m_i + \frac{q_0}{2}\right) + \sqrt{\left(m_i + \frac{q_0}{2}\right)^2 + \left(\frac{\sqrt{q^2 - q_0^2}}{2} - \frac{m_i q_0}{\sqrt{q^2 - q_0^2}}\right)^2} \quad (\text{A.30})$$

$$E_i^{t^+} = -\left(m_i + \frac{q_0}{2}\right) + \sqrt{\left(m_i + \frac{q_0}{2}\right)^2 - \left(\frac{\sqrt{q_0^2 - q^2}}{2} + \frac{m_i q_0}{\sqrt{q_0^2 - q^2}}\right)^2}. \quad (\text{A.31})$$

These are both the same root of Eq. A.15, but with an interchange of $t \leftrightarrow -t$. We denote the response function for $t < 0$ as S^- and for $t > 0$ as S^+ . For S^- we have

$$S_m^- = \alpha t^n \frac{m_i^2}{\pi q^{2m+1}} \sum_{r=0}^m \mathcal{V}_{m,r} \int_{E_i^{t^-}}^{\infty} dE_i E_i^r f_{\text{FD}}(E_i) (1 - f_{\text{FD}}(E_i + q_0)) \quad (\text{A.32})$$

$$= \alpha t^n \frac{m_i^2}{\pi q^{2m+1}} \sum_{r=0}^m \mathcal{V}_{m,r} \sum_{j=0}^r \binom{r}{j} \varepsilon_{F,i}^{r-j} \int_{E_i^{t^-}}^{\infty} dE_i (E_i - \varepsilon_{F,i})^j f_{\text{FD}}(E_i) f_{\text{FD}}(-E_i - q_0) \quad (\text{A.33})$$

$$= \alpha t^n \frac{m_i^2}{\pi q^{2m+1}} \sum_{r=0}^m \mathcal{V}_{m,r} \sum_{j=0}^r \binom{r}{j} \varepsilon_{F,i}^{r-j} \frac{(-1)^j q_0^{j+1}}{j+1} \left[1 - g_j \left(\frac{E_i^{t^-} - \varepsilon_{F,i}}{q_0} \right) \right] \quad (\text{A.34})$$

$$= \alpha t^n \frac{m_i^2}{\pi q^{2m+1}} \sum_{r=0}^m \mathcal{V}_{m,r} \sum_{j=0}^r \binom{r}{j} \varepsilon_{F,i}^{r-j} \frac{(-1)^j q_0^{j+1}}{j+1} h_j \left(\frac{E_i^{t^-} - \varepsilon_{F,i}}{q_0} \right), \quad (\text{A.35})$$

while for S^+ the logic is

$$S_m^+ = \alpha t^n \frac{m_i^2}{\pi q^{2m+1}} \sum_{r=0}^m \mathcal{V}_{m,r} \int_0^{E_i^{t^+}} dE_i E_i^r f_{\text{FD}}(E_i) (1 - f_{\text{FD}}(E_i + q_0)) \quad (\text{A.36})$$

$$= \alpha t^n \frac{m_i^2}{\pi q^{2m+1}} \sum_{r=0}^m \mathcal{V}_{m,r} \sum_{j=0}^r \binom{r}{j} \varepsilon_{F,i}^{r-j} \int_0^{E_i^{t^+}} dE_i (E_i - \varepsilon_{F,i})^j f_{\text{FD}}(E_i) f_{\text{FD}}(-E_i - q_0) \quad (\text{A.37})$$

$$= \alpha t^n \frac{m_i^2}{\pi q^{2m+1}} \sum_{r=0}^m \mathcal{V}_{m,r} \sum_{j=0}^r \binom{r}{j} \varepsilon_{F,i}^{r-j} \frac{(-1)^j q_0^{j+1}}{j+1} \left[g_j \left(\frac{E_i^{t^+} - \varepsilon_{F,i}}{q_0} \right) - g_j \left(\frac{-\varepsilon_{F,i}}{q_0} \right) \right] \quad (\text{A.38})$$

$$= -\alpha t^n \frac{m_i^2}{\pi q^{2m+1}} \sum_{r=0}^m \mathcal{V}_{m,r} \sum_{j=0}^r \binom{r}{j} \varepsilon_{F,i}^{r-j} \frac{(-1)^j q_0^{j+1}}{j+1} h_j \left(\frac{E_i^{t^+} - \varepsilon_{F,i}}{q_0} \right) \quad \text{for } q_0 < 0, \quad (\text{A.39})$$

with

$$h_j(x) = \begin{cases} 0, & x > 0 \\ (-x)^{j+1}, & -1 < x < 0 \\ 1, & x < -1 \end{cases} \quad (\text{A.40})$$

The final step of the S^+ calculation holds only for up-scattering of the DM, i.e. $q_0 < 0$.

For matrix elements that are polynomials in s and t , the full response function is simply the sum of the n and m , giving

$$S^- = \sum_{n,m} \alpha_{n,m} t^n \frac{m_i^2}{\pi q^{2m+1}} \sum_{r=0}^m \mathcal{V}_{m,r} \sum_{j=0}^r \binom{r}{j} \varepsilon_{F,i}^{r-j} \frac{(-1)^j q_0^{j+1}}{j+1} h_j \left(\frac{E_i^{t^-} - \varepsilon_{F,i}}{q_0} \right) \quad (\text{A.41})$$

$$S^+ = - \sum_{n,m} \alpha_{n,m} t^n \frac{m_i^2}{\pi q^{2m+1}} \sum_{r=0}^m \mathcal{V}_{m,r} \sum_{j=0}^r \binom{r}{j} \varepsilon_{F,i}^{r-j} \frac{(-1)^j q_0^{j+1}}{j+1} h_j \left(\frac{E_i^{t^+} - \varepsilon_{F,i}}{q_0} \right) \quad (\text{A.42})$$

A.2 Elsatic Scattering

A.2.1 Down-scattering Rate

Returning to the scattering rate, we first look at the case of down-scattering, where the DM loses energy, $q_0 > 0$. In this case, the interaction rate is given by

$$\begin{aligned} \Gamma^-(E_\chi) = & \int \frac{d \cos \theta_\chi k'^2 dk'}{64\pi^3 E_\chi E'_\chi} \Theta(E_\chi - q_0 - m_\chi) \Theta(q_0) \sum_{n,m} \frac{\alpha_{n,m} t^n}{q^{2m+1}} \\ & \times \sum_{r=0}^m \mathcal{V}_{m,r} \sum_{j=0}^r \binom{r}{j} \varepsilon_{F,i}^{r-j} \frac{(-1)^j q_0^{j+1}}{j+1} h_j \left(\frac{E_i^{t^-} - \varepsilon_{F,i}}{q_0} \right) \end{aligned} \quad (\text{A.43})$$

Change variables to q_0 and q through

$$q_0 = E_\chi - \sqrt{k'^2 + m_\chi^2}, \quad (\text{A.44})$$

$$q^2 = k^2 + k'^2 - 2kk' \cos \theta_\chi, \quad (\text{A.45})$$

$$\implies dk' d \cos \theta_\chi = \frac{E'_\chi q}{kk'^2} dq_0 dq \quad (\text{A.46})$$

To further simplify the notation we introduce $t_E = -t = q^2 - q_0^2$, $dq = dt_E/(2q)$, and exchange the q -integral for

$$\implies dk' d \cos \theta_\chi = \frac{E'_\chi}{2kk'^2} dq_0 dt_E, \quad (\text{A.47})$$

giving the interaction rate as

$$\begin{aligned} \Gamma^-(E_\chi) = & \frac{1}{128\pi^3 E_\chi k} \int_0^{E_\chi - m_\chi} dq_0 \int dt_E \sum_{n,m} \frac{\alpha_{n,m} (-1)^n t_E^n}{(t_E + q_0^2)^{m+\frac{1}{2}}} \\ & \times \sum_{r=0}^m \mathcal{V}_{m,r} \sum_{j=0}^r \binom{r}{j} \varepsilon_{F,i}^{r-j} \frac{(-1)^j q_0^{j+1}}{j+1} h_j \left(\frac{E_i^{t^-} - \varepsilon_{F,i}}{q_0} \right) \end{aligned} \quad (\text{A.48})$$

$$\begin{aligned} = & \sum_{n,m} \frac{(-1)^n \alpha_{n,m}}{128\pi^3 E_\chi k} \int_0^{E_\chi - m_\chi} dq_0 \int \frac{dt_E t_E^n}{(t_E + q_0^2)^{m+\frac{1}{2}}} \\ & \times \sum_{r=0}^m \mathcal{V}_{m,r} \sum_{j=0}^r \binom{r}{j} \varepsilon_{F,i}^{r-j} \frac{(-1)^j q_0^{j+1}}{j+1} h_j \left(\frac{E_i^{t^-} - \varepsilon_{F,i}}{q_0} \right). \end{aligned} \quad (\text{A.49})$$

There are then two main cases to consider; when $h_j(x)$ is unity or when it is not. We denote the t_E integrand in the former case as f_1 and f_2 for the latter, given explicitly as

$$f_1^{(m,n)}(t_E) = \frac{t_E^n}{(t_E + q_0^2)^{m+\frac{1}{2}}} \sum_{r=0}^m \mathcal{V}_{m,r} \sum_{j=0}^r \binom{r}{j} \varepsilon_{F,i}^{r-j} \frac{(-1)^j q_0^{j+1}}{j+1}, \quad (\text{A.50})$$

$$f_2^{(m,n)}(t_E) = \frac{-t_E^n}{(t_E + q_0^2)^{m+\frac{1}{2}}} \sum_{r=0}^m \mathcal{V}_{m,r} \sum_{j=0}^r \binom{r}{j} \varepsilon_{F,i}^{r-j} \frac{1}{j+1} \left(E_i^{t^-} - \varepsilon_{F,i} \right)^{j+1}, \quad (\text{A.51})$$

where we suppress the explicit dependence on the other variables for brevity. We encode the integrals over t_E within an operator

$$\begin{aligned} \mathcal{I}_{n,m}(f^{(m,n)}(t), t_1^+, t_2^+, t_1^-, t_2^-) &= \sum_{i=1,2} \sum_{j=1,2} \left(F^{(m,n)}(t_i^+) - F^{(m,n)}(t_j^-) \right) \\ &\quad \times \Theta(t_{3-i}^+ - t_i^+) \Theta(t_i^+ - t_j^-) \Theta(t_j^- - t_{3-j}^-), \end{aligned} \quad (\text{A.52})$$

$$F^{(m,n)}(t) = \int dt f^{(m,n)}(t). \quad (\text{A.53})$$

The full interaction rate is then written as

$$\begin{aligned} \Gamma^-(E_\chi) &= \sum_{n,m} \frac{(-1)^n \alpha_{n,m}}{128\pi^3 E_\chi k} \int_0^{E_\chi - m_\chi} dq_0 \\ &\quad \times \left[\mathcal{I}_{n,m} \left(f_1^{(m,n)}(t), t_E^+, t_{\mu^-}^+, t_E^-, t_{\mu^-}^- \right) \Theta(\varepsilon_{F,i} - q_0) \right. \\ &\quad + \mathcal{I}_{n,m} \left(f_2^{(m,n)}(t), t_E^+, t_{\mu^+}^+, t_E^-, t_{\mu^+}^- \right) \Theta(\varepsilon_{F,i} - q_0) \\ &\quad + \mathcal{I}_{n,m} \left(f_2^{(m,n)}(t), t_E^+, t_{\mu^-}^-, t_E^-, t_{\mu^+}^- \right) \Theta(\varepsilon_{F,i} - q_0) \\ &\quad \left. + \mathcal{I}_{n,m} \left(f_2^{(m,n)}(t), t_E^+, t_{\mu^+}^+, t_E^-, t_{\mu^+}^- \right) \Theta(q_0 - \varepsilon_{F,i}) \right], \end{aligned} \quad (\text{A.54})$$

where the t_E integration limits are

$$t_E^\pm = 2 \left[E_\chi(E_\chi - q_0) - m_\chi^2 \pm k \sqrt{(E_\chi - q_0)^2 - m_\chi^2} \right], \quad (\text{A.55})$$

$$\begin{aligned} t_{\mu^+}^\pm &= 2 [\varepsilon_{F,i}(\varepsilon_{F,i} + q_0) + m_i(2\varepsilon_{F,i} + q_0) \\ &\quad \pm \sqrt{(\varepsilon_{F,i}(\varepsilon_{F,i} + q_0) + m_i(2\varepsilon_{F,i} + q_0))^2 - m_i^2 q_0^2}], \end{aligned} \quad (\text{A.56})$$

$$\begin{aligned} t_{\mu^-}^\pm &= 2 [\varepsilon_{F,i}(\varepsilon_{F,i} - q_0) + m_i(2\varepsilon_{F,i} - q_0) \\ &\quad \pm \sqrt{(\varepsilon_{F,i}(\varepsilon_{F,i} - q_0) + m_i(2\varepsilon_{F,i} - q_0))^2 - m_i^2 q_0^2}], \end{aligned} \quad (\text{A.57})$$

All interaction rate spectra will have an endpoint at $q_0 = q_0^{\text{MAX}}$, the maximum amount of energy that can be lost in a single interaction. The value of q_0^{MAX} is shown in the left panel of Fig. 1.2 as a function of B in the case of large DM mass ($m_\chi = 1 \text{ TeV}$), for several values of $\varepsilon_{F,n}$. The endpoint can be found as the minimum between the DM kinetic energy and the root of one of the following two equations

$$t_E^- = t_{\mu^+}^+, \quad (\text{A.58})$$

$$t_E^+ = t_{\mu^+}^-. \quad (\text{A.59})$$

Only one of these equations will have a positive root for a given choice of m_χ , $\varepsilon_{F,n}$ and E_χ . For $m_\chi \gg m_i$, the second equation never has a solution, and the solution of the first equation is always much lower than the kinetic energy. This results in the value of q_0^{MAX} becoming independent of m_χ in this mass range.

The shape of the differential interaction rate depends very weakly on m_χ and B for $m_\chi \gg m_i$ and $m_\chi \ll m_i$, as seen by plotting it as a function of $q_0^{\text{norm}} = q_0/q_0^{\text{MAX}}$. Therefore, we use as a reference $m_\chi = 1 \text{ TeV}$ (left) and $m_\chi = 10 \text{ MeV}$ (right), $B = 0.5$, and show the normalised differential interaction rates in Fig. A.2 for $n = 0, 1, 2$, and neutron targets. We observe in the left panels that for $n = 0$ interaction rates are flat (or peaked, depending on $\varepsilon_{F,n}$) at low energy and suppressed at high energies, while for $n = 1, 2$ the profiles become peaked at higher and higher energies. Conversely, for $m_\chi = 10 \text{ MeV}$ the peak of the spectrum is shifted to lower energies with increasing power of t ($d\sigma \propto t^n$).

A.3 Up-scattering Rate

We now treat the case of $q_0 < 0$ applicable to up scattering and evaporation. Focusing on s -independent matrix elements for the moment, the response function is

$$S_{\text{up}}^-(q_0, q) = \frac{m_i^2}{\pi q} \int_{E_i^{t-}}^{\infty} f_{\text{FD}}(E_i) (1 - f_{\text{FD}}(E_i - |q_0|)) \quad (\text{A.60})$$

and evaluate the integral, now with $q_0 < 0$. If we attempt to take the $T_\star \rightarrow 0$ limit as before, we find that there is no overlap of the FD distributions and the result vanishes. Instead, we keep the leading order thermal corrections, i.e. terms of order $e^{-|q_0|/T_\star}$. The result is

$$\mathcal{F}_0(E_i, -|q_0|) = \frac{T_\star e^{-|q_0|/T_\star}}{1 - e^{-|q_0|/T_\star}} \left[\log \left(1 + e^{(E_i - \varepsilon_{F,i})/T_\star} \right) - \log \left(1 + e^{(E_i - |q_0| - \varepsilon_{F,i})/T_\star} \right) \right], \quad (\text{A.61})$$

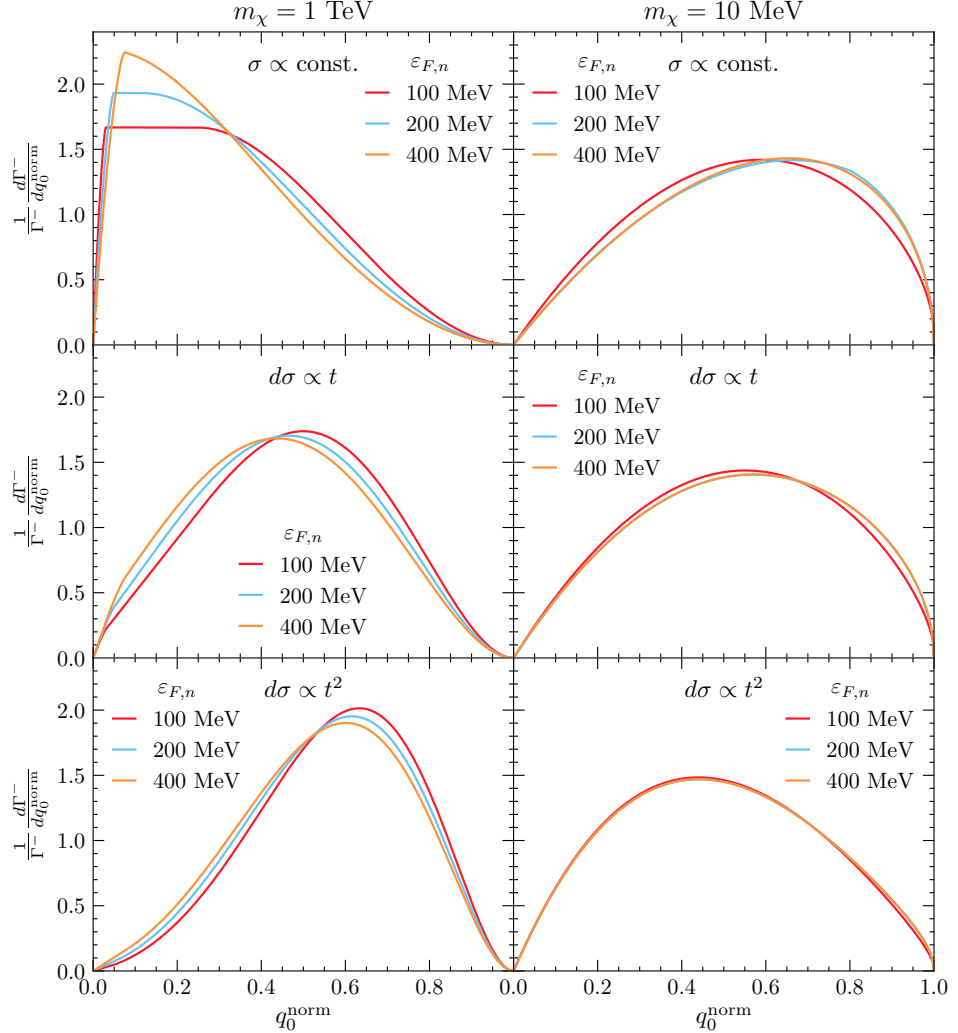


Figure A.2: Normalised differential interaction rates, $\frac{1}{\Gamma} \frac{d\Gamma^-}{dq_0^{\text{norm}}}$, as a function of q_0^{norm} for different values of $\varepsilon_{F,n}$, with $m_\chi = 1 \text{ TeV}$ (left panels) $m_\chi = 10 \text{ MeV}$ (right panels) and $B = 0.5$. Top row: $n = 0$, middle row: $n = 1$, bottom row: $n = 2$.

where after taking $T_\star \rightarrow 0$ we recognise three regions of interest

$$\lim_{T_\star \rightarrow 0} T_\star \mathcal{F}_0(E_i, -|q_0|) = \begin{cases} \frac{|q_0| e^{-|q_0|/T_\star}}{1 - e^{-|q_0|/T_\star}}, & E_i > \varepsilon_{F,i} + |q_0| \\ \frac{(E_i - \varepsilon_{F,i}) e^{-|q_0|/T_\star}}{1 - e^{-|q_0|/T_\star}}, & \varepsilon_{F,i} + |q_0| > E_i > \varepsilon_{F,i} \\ 0, & \varepsilon_{F,i} > E_i \end{cases} \quad (\text{A.62})$$

and we can write this as

$$\lim_{T_\star \rightarrow 0} T_\star \mathcal{F}_0(E_i, -|q_0|) = \frac{|q_0| e^{-|q_0|/T_\star}}{1 - e^{-|q_0|/T_\star}} h_0 \left(\frac{\varepsilon_{F,i} - E_i}{q_0} \right). \quad (\text{A.63})$$

The response function for upscattering is then

$$S_{\text{up}}^-(q_0, q) = \frac{m_i^2 q_0}{\pi q} \frac{e^{-|q_0|/T_\star}}{e^{-|q_0|/T_\star} - 1} \left[1 - h_0 \left(\frac{E_i^{t^-} - \varepsilon_{F,i}}{q_0} \right) \right] \quad (\text{A.64})$$

$$= \frac{m_i^2 q_0}{\pi q} \frac{e^{-|q_0|/T_\star}}{e^{-|q_0|/T_\star} - 1} g_0 \left(\frac{\varepsilon_{F,i} - E_i^{t^-}}{q_0} \right), \quad (\text{A.65})$$

leading to the corresponding up-scattering rate being

$$\Gamma_{\text{up}}^-(E_\chi) = \int \frac{k'^2 d \cos \theta dk'}{64\pi^2 m_i^2 E_\chi E'_\chi} |\bar{\mathcal{M}}|^2 \Theta(E_\chi + |q_0| - m_\chi) \Theta(q_0) S_{\text{up}}^-(q_0, q) \quad (\text{A.66})$$

$$= \frac{(-1)^n \alpha}{128\pi^3 E_\chi k} \int_{-\infty}^0 dq_0 \frac{q_0 e^{q_0/T_\star}}{e^{q_0/T_\star} - 1} \int dt_E \frac{t_E^n}{\sqrt{t_E - |q_0|^2}} g_0 \left(\frac{\varepsilon_{F,i} - E_i^{t^-}}{q_0} \right) \quad (\text{A.67})$$

where we have substituted $|\bar{\mathcal{M}}|^2 = \alpha t^n$ as the matrix element. Typically, we expect to be in the regime where $g_0 = 1$, and so the differential up-scattering rate is related result for down-scattering through

$$\frac{d\Gamma_{\text{up}}^-}{dq_0} = \frac{e^{-|q_0|/T_\star}}{e^{-|q_0|/T_\star} - 1} \frac{d\Gamma_{\text{down}}^-}{dq_0} \quad (\text{A.68})$$

This result applies generally to all matrix elements, not just the ones $\propto t^n$. The result can be derived from the principle of detailed balance, and hence is true for all interactions we consider. To calculate the total interaction rate, the t_E integrations can be performed in the same manner as in the previous section, with the q_0 integration bounds being $(-\infty, 0)$.

A.4 Interaction Rate for Low Energies

Need to consider the case where $T_\chi = E_\chi - m_\chi < \mu_F$, with $0 < q_0 < T_\chi < \varepsilon_{F,i}$. Then the t_E integration limits follow the hierarchy; $t_{\mu^+}^+ \sim t_{\mu^-}^+ \geq t_{\mu^-}^- \sim t_{\mu^+}^- \gtrsim 0$, and $t_{\mu^-}^+ \gg t_E^+ \geq t_E^- \gg t_{\mu^-}^-$. Then the only term in A.54 that remains is the first term, and only the $i = j = 1$ term contributes, leaving

$$\Gamma^-(E_\chi) = \sum_{n,m} \frac{(-1)^n \alpha_{n,m}}{128\pi^3 E_\chi k} \int_0^{E_\chi - m_\chi} dq_0 \int_{t_E^-}^{t_E^+} dt_E f_1^{(m,n)}(t_E) \quad (\text{A.69})$$

At first order in q_0 and K_χ , we have the following approximations

$$E_\chi \approx m_\chi \quad (\text{A.70})$$

$$k \approx \sqrt{2m_\chi T_\chi} \quad (\text{A.71})$$

$$t_E^\pm \approx 4m_\chi T_\chi \left[1 - \frac{q_0}{2K_\chi} \pm \sqrt{1 - \frac{q_0}{K_\chi}} \right] \quad (\text{A.72})$$

$$\Gamma^- \approx \sum_{n,m} \frac{(-1)^n \alpha_{n,m}}{128\sqrt{2}\pi^3 m_\chi^{3/2} K_\chi^{1/2}} \int_0^{K_\chi} dq_0 \int_{t_E^-}^{t_E^+} dt_E f_1^{(m,n)}(t_E) \quad (\text{A.73})$$

For single term matrix elements such that $|\bar{\mathcal{M}}|^2 = \alpha_{n,m}(-t)^n s^m$, the corresponding $\Gamma_{n,m}^-$ are

$$\Gamma_{0,0}^- = \frac{\alpha_{0,0}}{120\pi^3 m_\chi} K_\chi^2 \quad (\text{A.74})$$

$$\Gamma_{1,0}^- = \frac{2\alpha_{1,0}}{105\pi^3} K_\chi^3 \quad (\text{A.75})$$

$$\Gamma_{2,0}^- = \frac{4\alpha_{2,0} m_\chi}{63\pi^3} K_\chi^4 \quad (\text{A.76})$$

$$\Gamma_{0,1}^- = \frac{\alpha_{0,1}((m_i + m_\chi)^2 + 2m_\chi \varepsilon_{F,i})}{120\pi^3} K_\chi^2 \quad (\text{A.77})$$

$$\Gamma_{1,1}^- = \frac{2\alpha_{1,1}((m_i + m_\chi)^2 + 2m_\chi \varepsilon_{F,i})}{105\pi^3} K_\chi^3 \quad (\text{A.78})$$

$$\Gamma_{0,2}^- = \frac{\alpha_{0,2}((m_i + m_\chi)^2 + 2m_\chi \varepsilon_{F,i})^2}{120\pi^3} K_\chi^2 \quad (\text{A.79})$$

The $\alpha_{n,m}$ can be obtained at some reference point, taken to be the surface of the NS, from the differential cross-section,

$$\frac{d\sigma}{d\cos\theta} = \frac{\alpha_{n,m}(-t)^n s^m}{32\pi(m_i + m_\chi)^2} \quad (\text{A.80})$$

which gives

$$\sigma_{0,0} = \frac{\alpha_{0,0}}{16\pi(m_i + m_\chi)^2} \quad (\text{A.81})$$

$$\sigma_{1,0} = \frac{\alpha_{1,0}}{32\pi(m_i + m_\chi)^2} t_{max} \quad (\text{A.82})$$

$$\sigma_{2,0} = \frac{1}{3} \frac{\alpha_{2,0}}{16\pi(m_i + m_\chi)^2} t_{max}^2 \quad (\text{A.83})$$

$$\sigma_{0,1} = \frac{\alpha_{0,1}}{16\pi(m_i + m_\chi)^2} s \quad (\text{A.84})$$

$$\sigma_{1,1} = \frac{\alpha_{1,1}}{32\pi(m_i + m_\chi)^2} t_{max} s \quad (\text{A.85})$$

$$\sigma_{0,2} = \frac{\alpha_{0,2}}{16\pi(m_i + m_\chi)^2} s^2 \quad (\text{A.86})$$

where I have used

$$t = -\frac{t_{max}}{2}(1 - \cos \theta) \quad (\text{A.87})$$

$$t_{max} \sim \frac{4m_i^2 m_\chi^2}{(m_i^2 + m_\chi^2)} \frac{1 - B(R_\star)}{B(R_\star)} \quad (\text{A.88})$$

$$s \sim m_i^2 + m_\chi^2 + \frac{2m_\chi(m_i + \varepsilon_{F,i})}{\sqrt{B(R_\star)}} \quad (\text{A.89})$$

$$\sim (m_i + m_\chi)^2 \quad (\text{A.90})$$

Again introducing the correction

$$\zeta = \frac{n_n}{n_{free}} \sim \frac{3\pi^2}{(2m_i \varepsilon_{F,i})^{3/2}} n_n \quad (\text{A.91})$$

Then the interaction rates can be expressed with respect to the surface of the star

as

$$\Gamma_{0,0}^-(K_\chi) = \frac{\sqrt{2}}{10} \frac{(1+\mu)^2}{\mu} \frac{m_i}{(m_i \varepsilon_{F,i})^{3/2}} \sigma_{surf} n_n K_\chi^2 \quad (\text{A.92})$$

$$\Gamma_{1,0}^-(K_\chi) = \frac{4\sqrt{2}}{35} \frac{(1+\mu)^2(1+\mu^2)}{\mu^2} \frac{1}{(m_i \varepsilon_{F,i})^{3/2}} \frac{B(R_\star)}{(1-B(R_\star))} \sigma_{surf} n_n K_\chi^3 \quad (\text{A.93})$$

$$\Gamma_{2,0}^-(K_\chi) = \frac{\sqrt{2}}{7} \frac{(1+\mu)^2(1+\mu^2)^2}{\mu^3} \frac{1}{m_i(m_i \varepsilon_{F,i})^{3/2}} \left(\frac{B(R_\star)}{(1-B(R_\star))} \right)^2 \sigma_{surf} n_n K_\chi^4 \quad (\text{A.94})$$

$$\Gamma_{0,1}^-(K_\chi) = \frac{\sqrt{2}}{10} \frac{(m_i(1+\mu)^2 + 2\mu\varepsilon_{F,i})}{\mu(m_i \varepsilon_{F,i})^{3/2}} \sigma_{surf} n_n K_\chi^2 \quad (\text{A.95})$$

$$\Gamma_{1,1}^-(K_\chi) = \frac{4\sqrt{2}}{35} \frac{(m_i(1+\mu)^2 + 2\mu\varepsilon_{F,i})(1+\mu^2)}{\mu^2 m_i(m_i \varepsilon_{F,i})^{3/2}} \frac{B(R_\star)}{(1-B(R_\star))} \sigma_{surf} n_n K_\chi^3 \quad (\text{A.96})$$

$$\Gamma_{0,2}^-(K_\chi) = \frac{\sqrt{2}}{10} \frac{(m_i(\mu+1)^2 + 2\mu\varepsilon_{F,i})^2}{\mu(\mu+1)^2 m_i(\varepsilon_{F,i} m_i)^{3/2}} \sigma_{surf} n_n K_\chi^2 \quad (\text{A.97})$$

The average energy loss per collision is given by

$$\langle \Delta T \rangle = \frac{1}{\Gamma^-} \int_0^{K_\chi} dq_0 q_0 \frac{d\Gamma^-}{dq_0} \quad (\text{A.98})$$

which gives the results

$$\langle \Delta T^{0,0} \rangle = \frac{4}{7} K_\chi \sim \langle \Delta T^{0,1} \rangle \sim \langle \Delta T^{0,2} \rangle \quad (\text{A.99})$$

$$\langle \Delta T^{1,0} \rangle = \frac{5}{9} K_\chi \sim \langle \Delta T^{1,1} \rangle \quad (\text{A.100})$$

$$\langle \Delta T^{2,0} \rangle = \frac{28}{55} K_\chi \quad (\text{A.101})$$

The DM will reach thermal equilibrium with the targets when $K_\chi = T_\star$. There are two stages to this process; one where the interactions are not affected by Pauli blocking which takes N_1 collisions, and the next N_2 collisions where Pauli blocking is in effect. The time it takes for thermalisation to occur is given by the sum of the average times between collisions

$$t_{\text{therm}} = \sum_{n=0}^{N_2} \frac{1}{\Gamma^-(T_n)} \sim \sum_{n=N_1}^{N_2} \frac{1}{\Gamma^-(T_n)} \quad (\text{A.102})$$

where T_n is the DM kinetic energy after n collisions. If Pauli blocking is in effect for the entire process, then T_n is related to the initial kinetic energy, T_0 through

$$T_n = T_0 \left(1 - \frac{\Delta T}{T} \right)^n. \quad (\text{A.103})$$

This result implies the following relation;

$$\frac{T_N}{T_0} = \frac{T_{eq}}{T_0} = \left(1 - \frac{\Delta T}{T}\right)^N \quad (\text{A.104})$$

Then for interaction rates which follow $\Gamma^- \propto (K_\chi)^p$, we have that

$$t_{\text{therm}} \propto \sum_{n=N_1}^{N_2} (T_n)^{-p} \quad (\text{A.105})$$

$$= \frac{1}{T_{N_1}^p} \sum_{n=N_1}^{N_2} \left(\left(1 - \frac{\Delta T}{T}\right)^{-p} \right)^n \quad (\text{A.106})$$

$$= \frac{1}{T_{N_1}^p} \frac{(1 - \Delta T/T)^{p(1-N_1)} - (1 - \Delta T/T)^{-pN_2}}{-1 + (1 - \Delta T/T)^p} \quad (\text{A.107})$$

$$\sim \frac{1}{T_{N_1}^p} \frac{(1 - \Delta T/T)^{-pN_2}}{1 - (1 - \Delta T/T)^p} \quad \text{for } N_2 > N_1 \quad (\text{A.108})$$

$$= \frac{1}{T_{N_1}^p} \left(\frac{T_{eq}}{T_{N_1}} \right)^{-p} \frac{1}{1 - (1 - \Delta T/T)^p} \quad (\text{A.109})$$

$$= \frac{1}{T_{eq}^p} \frac{1}{1 - (1 - \Delta T/T)^p} \quad (\text{A.110})$$